Vilnius University
Faculty of Physics
Institute of Chemical Physics

Kamilė Kandrotaitė

SUBMICROMETER AEROSOL PARTICLES DYNAMICS IN AMBIENT AIR

Master's final thesis

Life and Chemical Physics study programme

Student	Kamilė Kandrotaitė
Approved	2024-05-22
Academic supervisor	dr. Vytautas Klimavičius
Consultant	dr. Lina Davulienė
Consultant	dr. Thomas Holst
Consultant	dr. Erik Ahlberg
Director of the Institute	prof. Darius Abramavičius

Vilnius 2024

Contents

Introduction

Air pollution is one of the world's leading risk factors for death. Studies suggests that aerosol particle pollution contributes to around 7 million premature deaths annually worldwide, thus ranking it as a primary cause of mortality globally [1, 2]. Aerosols are important in influencing health, given their effects on human respiratory systems and general well-being. Toxicological studies have shown that aerosol particles suspended in the atmosphere can carry significant health risks [3, 4]. Aerosols can penetrate deep into the human lungs due to their size and characteristics, impacting their deposition and absorption in the lung tissues [5]. Particles smaller than 5 μm have a high probability of deposition in the bronchial tree and alveoli, while ultrafine particles smaller than 100 nm, penetrate deeper in human lungs and are more efficiently absorbed in lung reaching cardiovascular system or bloodstream [6].

The diverse physical, chemical, and optical properties of aerosol particles, which vary depending on their sources and production mechanisms, contribute significantly to the uncertainty to climate models [7]. These aerosols include wildfire smoke, desert dust, sea spray, biogenic, and anthropogenic (human-made) particles that can come from industrial processes, vehicles, and various modes of combustion and then interact with sunlight in complex ways, influencing the Earth's climate and atmosphere [8]. This interaction includes both direct effects, such as scattering and absorbing sunlight, and indirect effects, as aerosols modify cloud properties and distribution. Most aerosol particles reflect sunlight, reducing the solar energy reaching Earth's surface. However, some particles are dark, absorbing sunlight, which can warm the surrounding atmosphere, leading to the evaporation of nearby cloud droplets, suppression of convection, and potential alteration of large-scale atmospheric circulations. Additionally, aerosols typically serve as nuclei for water molecules, facilitating the formation of cloud droplets in most circumstances [8].

The pivotal role of aerosols in atmospheric processes raises a question - how are these tiny aerosols formed? New particle formation (NPF) is a crucial process in the atmosphere that significantly contributes to the number concentration budget for particles. Investigating NPF provides insights into atmospheric processes, including the nucleation, condensation, coagulation and evaporation of submicrometer particles.

Analysing data from three different sites ranging from Vilnius (Lithuania; urban background) to Hyltemossa (southern Sweden; commercial forest) and Abisko (northern Sweden; sub-arctic wetland), suggests new approaches to compare size distribution of submicrometer particles and new particle formation events. Such comparison for Nordic countries has not yet been carried out. By comparing size distribution, it is also advantageous to look into seasonality, patterns, different processes that can vary between different site types as well as locations. By analyzing aerosol properties, new particle formation events, and instrument performance, this thesis aims to provide insights into the factors influencing aerosol dynamics and provide spatial variability and different environments comparison.

The aim of this work is to analyse the sub-micrometer aerosol particle size distribution data and its dynamics measured in Vilnius urban background site (Lithuania) and to compare it with data from Swedish remote-rural sites, including the Hyltemossa and Abisko measurement station.

In order to achieve this goal the following objectives were formulated:

1. gain insights into instrument performance and data consistency by comparing different aerosol measurement instruments for critical aerosol properties (at Hyltemossa measurement station);
2. identify the formation of new aerosol particles and quantify the frequency and growth rates of new particle formation events measured in different regions during the campaign ;
3. analyse and identify the formation influencing factors of new aerosol particles;
4. compare various patterns of submicrometer aerosol particle concentration between measurement sites located in different regions and representing different background (i.e. urban, rural background, remote area).

1 Literature review

There is a growing focus on aerosol research, given their potential negative consequences for quality of life in various ways, including impacts on health, climate and ecosystems [8, 9]. Aerosol particles affect the optical properties of the atmosphere, such as light scattering and absorption, which determine visibility and affect the energy balance of the atmosphere [8]. Aerosol particles are known as hazardous atmospheric pollutants, and interest in their effects on human health is constantly increasing [10, 11]. The effect of aerosol particles on atmospheric properties and human health depends on their size, concentration and chemical composition [11].

Depending on their physical properties, different aerosols scatter or absorb sunlight shortwave radiation to varying degrees. Scattering aerosols contribute to cooling by increasing total reflected solar radiation, whereas heavily absorbing aerosols, such as black carbon (BC), contribute to warming, affecting the natural thermal balance [12]. The net impact on Earth's energy balance depends on surface and cloud characteristics. Aerosols are necessary for cloud formation, serving as cloud condensation nuclei (CCN) and ice nuclei [13]. Increased aerosol concentrations can lead to more cloud droplets, increasing cloud albedo and causing a a cooling effect, known as the cloud albedo effect [14]. Absorbing aerosols, such as BC, can modify cloud properties through indirect effects, impacting atmospheric stability, convection, and cloud formation [8]. Furthermore, absorbing aerosols deposited on snow or ice surfaces reduce surface albedo, leading to decreased reflectance of solar radiation and a heating effect [15]. Thus, aerosol particles has impact on global scale by absorption or scattering properties and cloud formation.

The World Health Organization's global air quality guidelines specify mass concentration limits for aerosol particles, such as particulate matter PM10, PM2.5, and PM1, but do not include any limits for number concentration [16]. However, the contribution of sub-micron size particles (less than 1 μm) to the mass concentration is very small compared to their surface area concentration due to the high number concentration [13]. This makes PM1 significantly more toxic than larger ones, as they pass unhindered through the airways to the alveoli of the lungs and enter the bloodstream along with the pathogens they contain [17]. This can cause adverse health effects ranging from simple short-term respiratory distress to cardiovascular and respiratory mortality system diseases and morbidity, lung cancer, brain diseases and mutagenic or carcinogenic effects [9, 18]. In order to reduce the negative impact of aerosol particles on human health and climate, it is necessary to study and understand the mechanisms determining the formation and abundance of these particles.

1.1 Classification of aerosol particles

Atmospheric aerosol particles are defined as a dispersed system composed of gases and solid or liquid particles suspended in the air [19]. Aerosol particles can be classified based on size, geometric shape, chemical composition, formation mechanism, etc. There are no strict classifications, which usually depend on the study or context, but the following terms are commonly used:

- Primary aerosol particles - particles that enter the ambient air from a source without undergoing chemical changes.

- Secondary aerosol particles - particles formed due to the oxidation of volatile organic compounds.

Particle size is one of the most important parameters when studying their behavior in a gas phase. Classification based on size includes: submicron (diameter < 1 μm) particles (PM1), supermicron (> 1 μm) particles, fine particles (< 2.5 μm) (PM2.5), coarse particles (> 2.5 μm). In scientific research, aerosol particles are often classified into different types called modes: accumulation mode (from 0.1 to 1–2 μm), Aitken mode (0.025–0.1 μm), nucleation mode (<0.025 μm). The finest particles are formed during gas phase nucleation processes when molecules cluster and form stable clusters. Particles formed during nucleation can grow due to condensational growth - non-volatile compounds condense onto particle nuclei [8]. Due to condensation processes, the grown particles further coagulate and, as they grow larger, supplement the accumulation mode. Accumulation mode particles can persist in the atmosphere for a long time (7-30 days) due to their low gravitational settling velocity and slow coagulation [6, 8]. In urban environments, nucleation and Aitken mode particles typically dominate aerosol particle number concentration and size distribution due to primary pollution sources such as fuel combustion for energy needs, transportation, and industrial activities [20].

1.2 Sources and dynamics of aerosol particles

The process by which secondary particles are formed is called nucleation. There are two different types of nucleation:

1. Heterogeneous nucleation - particle growth where vapor particles condense onto solid-phase aerosol particles;

2. Homogeneous nucleation - the process of forming new aerosol particles when sulfur dioxide (SO_2) oxidizes in the atmosphere to form sulfuric acid (H_2SO_4). This H_2SO_4 can react with water vapor (binary nucleation) or with water vapor and ammonia (ternary nucleation), forming droplets of sulfate solution [13].

M. Kulmala describes the formation of atmospheric aerosols in his studies as a two-stage process [21, 22]. In the first stage, the formation of stable clusters occurs. The size of clusters increases by condensing sulfuric acid and stabilizing with amines, ammonia, or organic vapors. The second stage is characterized by an increased rate of cluster growth due to activation by organic vapors. The dynamics of the aerosol system are defined by processes that determine the formation, growth, and losses of aerosol particles.

2 Methods

This thesis study focused on three different areas in North and North-eastern Europe (Sweden and Lithuania). All locations differ in site type: Vilnius (Lithunaia) was considered as urban background site, Hyltemossa (south of Sweden) represented a a forested and rural region, and Abisko (north of Sweden) was considered as a remote site located in sub-arctic region. Comparing different measurement sites and location gives insights into seasonality, patterns, different processes that can vary between them. This kind of comparison including data from Vilnius has not been done before.

Site and measurements description:

1. Vilnius, Lithuania. Measurements were conducted in the Center for Physical Sciences and Technology, Vilnius air pollution research site (54°43'21"N, 25°19'33"E). This site is considered representative of Vilnius urban background, since it is located around 7 km from the city centre and 0.3 km from the nearest urban road, with a forested area in between. The data was collected from March 2022 to February 2023, except September 2022 due to technical issues. The size distribution of submicron particles (10–800 nm) in the ambient air was measured using a Scanning Mobility Particle Sizer Spectrometer, which consists of a condensation particle counter (TSI model 3750) for particle counting and a differential mobility analyzer (TSI model 3083) for particle sizing.

2. Hyltemossa, Sweden. Hyltemossa Research Station is located in the northwestern Scania region (56°06'N, 13°25'E), in a managed spruce forest in southern Sweden. In this analysis, five instruments were used: Mobility Particle Size Spectrometer, Cloud Condensation Nuclei Counter, Fine Dust Monitor System, Aethalometer, and Aerosol Chemical Speciation Monitor. Study period: May 5, 2022, to April 30, 2023. The research station is included in the Aerosol, Clouds and Trace Gases Research Infrastructure (ACTRIS) and the Integrated Carbon Observation System (ICOS) networks.

3. Abisko, Sweden. Measurements were done at the Abisko Scientific Research Station (68°20'N 19°02'E) in the sub-Arctic area at the Stordalen mire complex. The surrounding Abisko area is dominated by birch forests. The site is located in a valley with mountains to the north and to the south, resulting in winds, and thus aerosol transport, primarily from the east and west. Both a Scanning Mobility Particle Sizer and an Air Ion Spectrometer were deployed to measure paricle size distribution during summer of 2023. This research station is included in ICOS network.

2.1 Instrumentation

To reach the aims, data on aerosol particle number, volume and mass concentration and size distribution is important which can be measured with the following instrumentation.

2.1.1 Mobility Particle Size Spectrometer

Mobility Particle Size Spectrometer (MPSS) is a measurement instrument based on electrical mobility properties of aerosol particles. MPSS is the most often used equipment for measuring the size distributions of ultrafine and fine aerosol particles in real time, with detected particle sizes ranging from 5 to 840 nm. Basic working principle of Scanning Mobility Particle Sizer (SMPS) and Mobility Particle Size Spectrometer is the same.

The main components of a typical MPSS include an ionising source (bipolar diffusion charger); a DMA (Differential Mobility Analyser) to classify the aerosol particles; a CPC (Condensation Particle Counter); a computer connected to the CPC to control the DMA + CPC, and to record the data; a signal connection from the CPC to the DMA that controls the DMA voltage [13].

Initially, the aerosol flow passes through an inertial impactor to remove particles larger than 10 μm. A bipolar diffusion charger (radioactive source of ^{63}Ni) gives the particles a uniform and known charge distribution, defined as bipolar charge equilibrium or Boltzmann equilibrium charge distribution [13]. After electrical charging in a bipolar diffusion charger, aerosol particles are classified by their electrical mobility in the electric field of a cylindrical capacitor DMA. The DMA, with a central rod controlling voltage between 20 and 10,000 V, creates an electrical field inside [23]. Near the bottom of the tube, there is a small gap that allows only specific particles with a certain electrical mobility (nearly monodisperse) to pass through and exit the classifier. The size is controlled by adjusting the voltage of the central rod. Smaller particles have a higher mobility and are directed towards the center of the flow, while larger particles move towards the periphery. The DMA allows for the characterization of particle size distribution by separating particles based on their electrical mobility [24]:

$$Z_p = \frac{n_e e C_c}{3\pi\eta d_p} \tag{1}$$

Here, n_e is the number of negative charges, C_c - size-dependent Cunningham slip correction factor, η - viscosity of the carrier gas, d_p - aerosol particle diameter. Then the sample flow is led directly to a CPC to detect and count the classified particles. Inside, the aerosol encounters a supersaturated vapor (butanol) that saturates particles [23]. It is then cooled by flowing through a cold tube to achieve the level of supersaturation required for particle growth. These droplets grow to a size that can be detected by the CPC's sensing mechanism through the scattering of light pulses [13]. The signals from the CPC are processed and analyzed to generate a size distribution profile of the particles in the sample. This data provides information on the number concentration of particles at different size ranges.

2.1.2 Cloud Condensation Nuclei Counter

The primary purpose of a Cloud Condensation Nuclei counter (CCNC) is to measure the concentration of aerosol particles in the atmosphere that can serve as nuclei for cloud droplet formation, known as Cloud Condensation Nuclei (CCN). These particles are critical in the initial stages of cloud formation, as they provide surfaces upon which water vapor can condense to form cloud

droplets. The principle of operation of a CCN counter is based on creating supersaturation conditions in a controlled environment and monitoring the ability of aerosol particles to act as nuclei for water droplet formation.

The main part of CCNC is the CCN growth chamber. In this chamber, that is a vertical column, continuous temperature gradient is achieved in the streamwise direction along the wetted surface [25]. While the laminar flow of aerosol passes through the column, both heat and water vapor move from the inner surface toward the tube's center. Due to the faster diffusion of water molecules compared to heat, a consistent supersaturation of water vapor forms along the central axis of the column [26]. Under supersaturated (SS) conditions, water vapor molecules start to condense onto aerosol particles, forming tiny water droplets. The supersaturation rate changes continuously to examine the conditions under which CCN activates. In this project, the maximum SS level was chosen (SS > 1), ensuring activation of all aerosol particles. This approach allowed for the extraction of the total number concentration that the CCNC can register. Activated droplet counting is done with an Optical Particle Counter (OPC). The OPC uses side-scattering for the particle sizing within the range of 0.75–10 μm [27].

However, not all aerosol particles can serve as effective CCN. CCN activity is controlled by size (Kelvin effect) and composition (Raoult effect). The Kelvin effect posits that the equilibrium vapor pressure is higher over a curved surface than a flat one due to reduced intermolecular forces. Smaller particles are more affected by curvature, and larger particles activate at lower supersaturations. On the other hand, Raoult's law provides insights into aerosol composition, stating that the water equilibrium vapor pressure is lower over a salt solution than pure water. In general, dependence of supersaturation on particle size can be described by Kohler equation [13], that incorporates both parameters: particle size and composition dependence.

2.1.3 Fine Dust Monitor System

The Fine Dust Monitor System (FIDAS) is an instrument designed to measure the concentration of fine particulate matter (PM), including PM1, PM2.5 and PM10 in ambient air. FIDAS operates based on optical particle measurement, using a combination of light scattering. The FIDAS system draws in ambient air samples through an inlet. When a particle passes through the laser beam, it scatters light in various directions. The amount and angle of light scattering are related to the size of the particle, with larger particles scattering more light and at wider angles. The instrument's software processes the data obtained from the detectors to generate a detailed particle size distribution [28]. The FIDAS instrument was not employed at Hyltemossa Station until January 2023; however, it was operational nearby (20 km to the west of Hyltemossa), representing a similar environment.

2.1.4 Aethalometer AE33

The Aethalometer is an optical measurement technique employed for assessing the concentration of optically-absorbing aerosols. The main operating principle of the Aetalometer is the increase in optical absorption with increasing concentration of aerosol particles containing Black Carbon (BC) on the filter.

The Aethalometer measures the intensity of light that has passed through a filter, where a sample is continuously collected, alongside a control region (where no sample is collected). In the initial section of the filter, sample deposition occurs, leading to a decrease in light absorption intensity due to the presence of deposited particles [29]. Consequently, the difference in light intensities between these two regions is directly proportional to the black carbon mass concentration. The analysis adheres to the Beer-Lambert law, establishing a relationship between light attenuation and the properties of the material through which the light passes. This evaluation covers seven optical wavelengths ranging from near-infrared to near-ultraviolet. Channel 6, measuring at a wavelength of 880 nm, is particularly significant as the standard for reporting BC concentration [30].

2.1.5 Aerosol Chemical Speciation Monitor

The Aerosol Chemical Speciation Monitor (ACSM) measures mass loading and chemical composition of non-refractory aerosol particles in real-time. Main ACSM application is ambient monitoring of NO_3, SO_4, NH_4, Cl and organic mass concentrations of aerosols, with aerodynamic diameters between 70 and 700 nm [31].

The instrument comprises the aerosol inlet and the particle composition detection section [32]. A narrow particle beam is created by the aerodynamic lens and transmitted into the detection chamber. Non-refractory aerosol components undergo rapid vaporization upon impacting a hot surface (600C) under high vacuum conditions (10^5Pa). Vaporized aerosol species are ionized by electron impact (EI) and then analyzed using mass spectrometry providing information about chemical composition [33].

2.1.6 Air Ion Spectrometer

The Air Ion Spectrometer (AIS) is a crucial tool for studying aerosols' effects on air quality, climate, precipitation, cloud formation, and pollution levels, as well as their broader environmental consequences [34]. It also explores the relationship between air ions and human health [35], providing valuable insights into aerosol properties by precisely measuring the concentration and size distribution of charged particles or atmospheric ions [36].

The AIS operates by detecting and measuring charged particles in the air based on their electric mobility perpendicular to the airflow [37]. Its design allows for the measurement of ion distributions of both polarities within a wide range of sizes, from molecular clusters of 0.80 nm to aerosol particles of 40 nm in diameter [34].

The AIS system consists of two identical cylindrical mobility analyzers, each comprising 21 measuring channels, totaling 42 channels for the spectrometer [34]. Air with ions is drawn into the analyzers through electronically controlled active electric filters, ensuring that the properties of the sampled air and the sheath air remain nearly identical [37]. The electric currents generated by ion fluxes across the mobility analyzer sections are measured by electrometers, forming the output signals of the instrument [37].

To mitigate the impact of parasitic currents and electrometer drift, the input signals are periodically disrupted by regulating the charging and electric filtration of particles in the input air [34].

Random measurement uncertainties are derived from these records, and the measurement process is controlled by a personal computer via the AIS controller, verifying the device's parameters during each measurement cycle [37].

2.2 Quality assurance, data analysis

In the Hyltemossa project, one of the aim was to do closure studies for quality assurance. This project involved comparing data obtained from different instruments focusing on total number concentration and PM1 mass concentration. Initially, the data was filtered to remove instances of malfunction based on logbooks that record instrument service problems, connection issues or calibration dates. Then data was filtered based on MPSS data availability covering the period from May 5, 2022, to April 30, 2023, in order to represent and analyze variations over the course of a year. This specific date range was applied uniformly to all the data (Hyltemossa), given that MPSS served as the primary instrument for comparison with other instruments regarding number and mass concentration. The following comparisons were chosen:

- CCNC (maximum SS) vs MPSS number concentration variation.
- FIDAS PM1 mass concentration vs MPSS volume concentration.
- ACSM and Athalometer mass concentration vs MPSS volume concentration.
- FIDAS PM1 vs ACSM and Athalometer mass concentration

It was chosen to compare data by plotting time-series, analyzing fractions or investigating correlations. Based on problems observed during different instrument intercomparison or metadata of the instruments, such as flow rate failures, issues with status, or unstable relative ionization efficiency, the data then underwent a second cleaning process.

Furthermore, mass concentration for MPSS was obtained by multiplying MPSS volume concentration by density. Density was calculated using ACSM and Aethalomether mass concentration dataset, according to the formula [38]:

$$\rho = \frac{Total_{ACSM} + eBC}{\frac{NO_3^-}{1.75} + \frac{SO_4^{2-}}{1.75} + \frac{NH_4^+}{1.75} + \frac{Cl^-}{1.52} + \frac{Org}{1.2} + \frac{eBC}{1.77}} \tag{2}$$

2.3 Identification of new particle formation

New Particle Formation (NPF) events, characterized by the emergence and growth of aerosol particles, are identified through a 'banana-shaped' pattern in size distribution graphs. Defined as 'NPF event days,' these are days when a new particle mode emerges, persists for over an hour, and shows signs of growth, typically below 25 nm [39].

According to Dal Maso et al [39] proposed classification scheme, new particle formation was classified into three categories: 'Event', where the NPF events is observable, growth rates is identified, 'Non-event', when where is no observable NPF and days that did not meet the criteria for event or non-event days were identified as undefined.

This classification method is typically used in remote environments where there are no polluted air masses [40]. Factors in polluted urban environments are more complex because primary pollution sources due to human activities (i.e., transportation, residential heating) occur daily [9]. Thus, a higher concentration of nucleation mode particles in the examined city of Vilnius may not necessarily indicate the formation of new particles but may also arise from local pollution sources. In this study, fluctuations in size distribution due to human activity were not analyzed because during nucleation development, there is no particle growth. During peak hours on working days – in the morning (from 06:00 to 09:00) and in the evening (from 18:00 to 21:00) due to heavy traffic from transportation and residential heating, a clear peak in the nucleation mode was clearly identified, which in Vilnius site is classified as non-event, even if increased nucleation mode formation may last longer than an hour.

The strength of NPF events is quantified Growth Rate (GR) [41]. The GR calculation involves determining the rate of change of particle radius (r) and time t required for banana shape growth:

$$GR = \frac{dr}{dt} \tag{3}$$

This approach involves a manual process. A linear fit is applied to interactively selected points, yielding the slope of the line, and resulting coefficient is provided in nm/h units. This approach offers an empirical determination of the growth rate for each NPF event [42].

2.4 Used statistics

In this work, several statistical methods was used for understanding relationship between two variables. Among them, in physics widely used the linear Pearson and Spearman's correlation were applied [43]. The Pearson correlation coefficient evaluates the linear connection between two continuous variables, assuming linearity in their relationship, normal distribution of the variables, and absence of significant outliers in the data. On the other hand, Spearman's correlation is used for assessing the monotonic relationship between continues or ordinal variables and demonstrates greater resilience to outliers [44]. Monotonic relationships differ from linear relationships in that the two variables might converge, but not at a constant rate [44]. Both the Pearson and Spearman correlation coefficients serve to measure the strength and direction of the relationship between two variables, yet they vary in the type of relationship they can detect, making them both valuable tools in statistical data analysis [43].

Another method used was the bootstrap method - a statistical method that uses random sampling with replacement to assign measures of accuracy such as bias, variance, confidence intervals, and prediction error to sample estimates [45]. This statistical technique involves resampling a single dataset to generate numerous simulated samples [46]. In this study, the bootstrap method is used to construct statistical confidence intervals and calculate 25 % and 75% percentiles (first and third quartiles).

Moreover, for closure study it was used more parameters mostly describing Pearson linear re-

lationship:

- correlation coefficient (r) - measure the strength and direction of the linear relationship.
- r-squared value (R^2) - measures the proportion of variance in the dependent variable that is predictable from the independent variables.
- slope (b) - indicates the average change in the dependent variable for a one-unit change in the independent variable [43].

The Hybrid Single-particle Lagrangian Integrated Trajectory (HYSPLIT) model [47] was applied to analyze backward air mass trajectories for Vilnius data. Air mass trajectories were computed using the HYSPLIT 4 model, which integrates the position of air masses over time [48]. The HYSPLIT model is widely recognized for its application in back trajectory analysis, particularly for determining the origins of air masses, as was done in this study. For the investigation of the air mass origin, the 18-h backward air trajectories arriving at the Vilnius site during case study (March 29 - April 2, 2022) were calculated using the HYSPLIT model. The default arrival height chosen for the analysis was 500 m above ground level. The trajectory was estimated for every 12 hour (2 trajectories per day) (Fig. 4).

3 Results and Discussion

3.1 Vilnius, Lithuania

3.1.1 New particle formation events in Vilnius

A total of 278 days were analyzed from March 2022 to February 2023. During the entire period, there were 95 days with new aerosol particle formation events and 135 days with no observed events (non-event days), with 48 cases classified as undefined. Most days with nucleation episodes (Fig. 1) were identified in spring and summer (over 40%), with peak in June (59 %), while non-event days tended to occur during the cold season (October-February) (around 40-70%). More frequent particle formation episodes during warmer periods were associated with higher temperatures, which accelerate photochemical processes [49]. According to seasonality, the recurrence of nucleation episodes exhibits similar trends in other European sites, with particle formation events prevailing in spring, summer, and early autumn seasons [40,50,51]. A high seasonal event frequency in spring and summer has been observed in different environmental locations with around 40% nucleation episodes during spring and summer months in Po Valley, Italy [52], Prague, Czech republic and Budapest, Hungary [50].

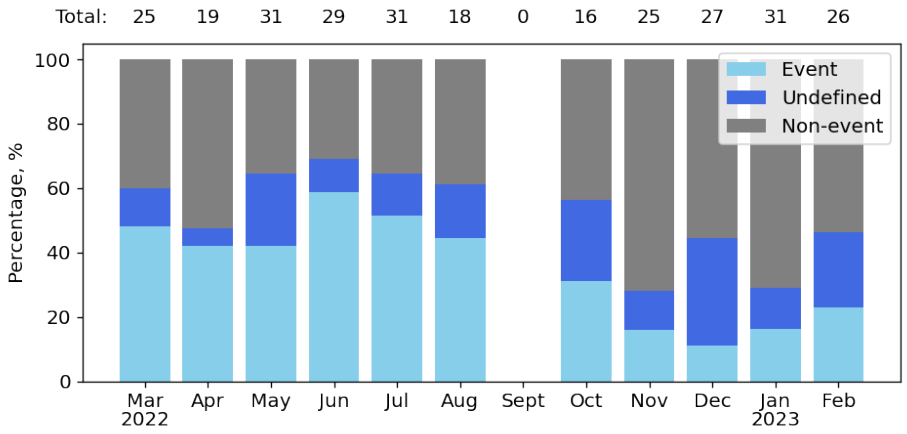

Fig. 1 Frequency of new particle formation event occurrence from March, 2022 to February, 2023 in Vilnius, Lithuania

3.1.2 Parametrization of new particle formation events

To assess the characteristics of new particle formation throughout the year, parameters such as growth rate (GR) were investigated, and their monthly average values are presented in Fig. 2. The calculated growth rates ranged from 0.7 to 20.1 nm/h, with the highest monthly values observed during June (average GR 9.3 nm/h). The lowest monthly growth rates occurred during the spring season, specifically in March (average GR 3.6 nm/h), and and in autumn, particularly in October (average GR 3.2 nm/h). However, it should be noted that there were fewer available days for calculating growth rates in October overall (16 days in total), which could explain the fluctuations in growth rate tendencies. It could be observed that during summer (average GR 8.6 nm/h), autumn

(average GR 5.4 nm/h) and winter (average GR 6.6 nm/h), the growth rates tended to be higher compared to the spring season (average GR 3.9 nm/h). Furthermore, it is evident that during warmer seasons, the data tended to exhibit a narrower range of distribution (standard deviation (SD) varies 1.8-4.7 nm/h) with occasional outliers. In contrast, during colder seasons, growth rates showed a wider variability (SD varies 5.1-6.6 nm/h, with exception in January 1.9 and October 0.9), suggesting a reduced stability in new particle growth. It can be observed that during the spring season, the growth rate was the lowest, indicating that aerosol particle size increases more slowly compared to other seasons [53].

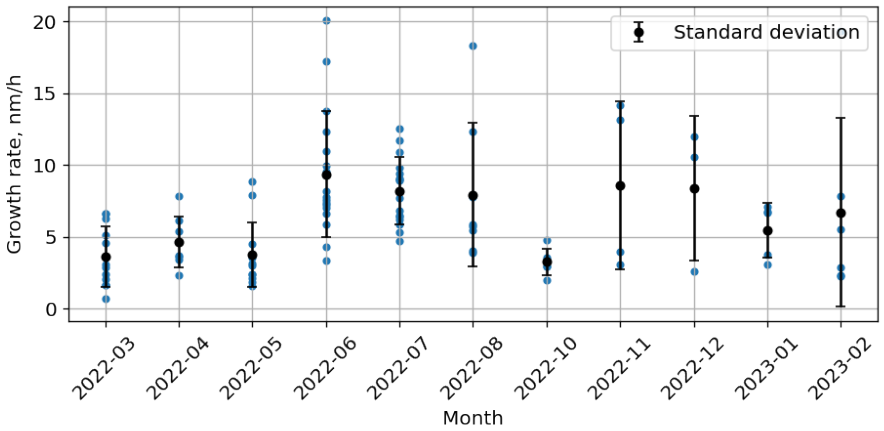

Fig. 2 Daily growth rates of new particle formation alongside monthly averages and standard deviation from March, 2022 to February, 2023 (Vilnius, Lithuania).

In Lithuania, few studies have investigated new particle formation in non-urban regions (Table 2), particularly at the Preila (coastal environment) and Rugsteliskis (forest environment) stations [42, 54]. In Vilnius, the average annual growth rate was calculated to be 6.4 nm/h, a value noticeably higher compared to those observed in Lithuanian coastal or forest environments. In those environments either winter seasons were not included or no new particle formation was observed. Conversely, in Vilnius, the growth rate fluctuates during the winter season, exhibiting higher values. This disparity could explain the considerable difference observed between these locations. Additionally, as Vilnius station is located in the suburb of the largest city of Lithuania, it is expected that the growth rate would be higher compared to rural sites [51]. Higher growth rates in urban environments could be associated with the presence of anthropogenic compounds [55]. Compared with other European locations based on studies in the literature [51], it was found that the median growth rate value in Vilnius (around 5.8 nm/h) could be characterized as indicative of an urban environment (Table 3, urban environment growth rate median value 5.9 nm/h).

Table 1 New particle formation characterization in environmental pollution research stations in Lithuania [42, 54].

Location	GR mean, nm/h
Preila [42]	3.8
Rūgšteliškis [54]	2.9
Vilnius (this work)	6.4

Table 2 Growth rate of new particle formation according to site type [53].

	Growth rate, nm/h		
Site type	5%	median	95%
Boreal	0.5	2.7	5.3
Remote or rural	2	3.5	9.6
Urban	4	5.9	12
Vilnius (this work)	1.8	5.8	14.3

3.1.3 Case study analysis

For further analysis, a sequence of three-day new particle formation events was chosen, from March 29 to March 31. Additionally, April 1 (Friday), representing a non-episodic day when no new particle formation was detected, and April 2 (Saturday), when a particle formation episode was observed again, were included. All new particle formation events are characterized by clearly defined banana shapes, where newly formed particles grow to the accumulation mode. The temporal evolution of these events is depicted in Fig. 3. These days were chosen for examination due to the typical workweek and changes in emissions.

In the morning, a spike in particle concentration (up to about 100 nm) was observed when traffic typically peaks, from 6 to 8 o'clock, until the morning traffic congestion ends. This morning concentration increase was observed on all weekdays, while on April 2 (Saturday), there was no such morning intensity, indicating reduced pollution levels due to lower traffic in the city. New partcile formation began between 12-15 o'clock, when N_{Nuc} increased to 5.2×10^3 cm^{-3} (March 29, 2022), 4.5×10^3 cm^{-3} (March 30, 2022), 3.9×10^3 cm^{-3} (March 31, 2022), and 6.9×10^3 cm^{-3} (April 2, 2022). Then, newly formed particles grew to 60-80 nm in size (Aitken mode, N_{Ait}), reaching numerical concentrations of up to 5×10^3 cm^{-3}, followed immediately by sharp increases in total concentration (N_{total}). These concentration enhancements, which last until nightfall, could be related to evening rush hours and residential heating processes. In contrast, on April 1, there were no signs of new particle formation, only morning and evening peaks were observed. Therefore, the concentration changes in such graphs enable monitoring of new particle formation, changes in particle concentration, and particle size variation.

The occurrence of observed aerosol particle formation events depended on meteorological conditions [53] (Fig. 3). Meteorological parameters show that throughout the 5 observed days, the minimum temperature of -5 °C was recorded at night, while higher temperatures reached about 2-6

°C at midday, leading to a corresponding decrease in relative humidity during this warmer part of the day. The lowest fluctuations in relative humidity, 38-45%, were observed on April 1. The wind mostly blew from the north, northwest, or northeast at speeds ranging from 1 to 6 m/s. It was noted that on April 1, a day without new particle formation, humidity remained relatively stable (SD = 2.5 %), whereas on the remaining days, humidity varied noticeably (SD ranging from 8% to 27%), particularly around midday showed a decreasing trend, coinciding with the onset of observed particle formation episodes.

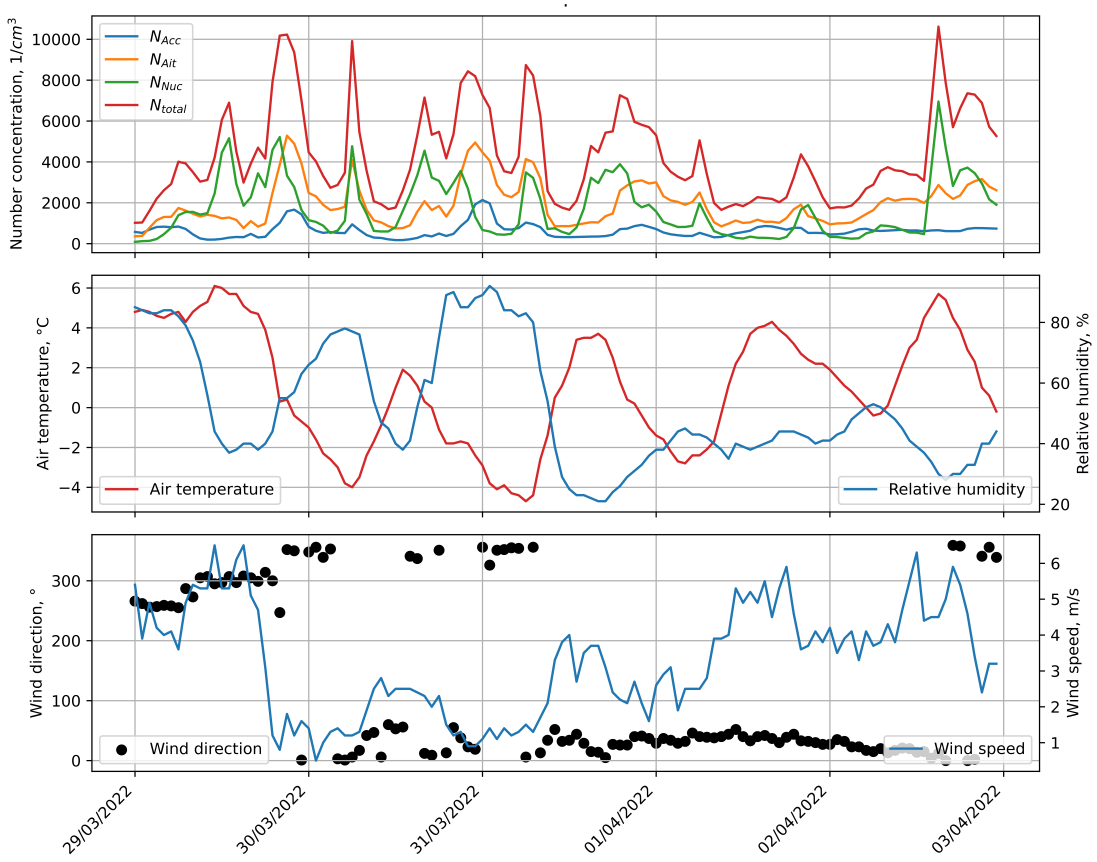

Fig. 3 From March 29 to April 2, 2022, temporal sequences of concentrations, relative humidity and temperature, wind speed and direction of individual aerosol particle modes (Vilnius, Lithuania).

To analyze and monitor the main sources of aerosols arriving to Vilnius, the NOAA HYSPLIT4 model for backward trajectories analysis was used [47] and observations are shown in Fig. 4. The most of the trajectories from March 27th to April 2nd was originating from the northern and western directions of the Baltic Sea region. Starting in the Baltic sea, air masses were transported through the Baltic countries. These air masses could be influenced by shipping emissions, as there is evidence of intensive ship activity in the Baltic sea [56, 57]. Additionally, studies suggest that air masses coming from the Baltic sea do not increase the pollution burden and are cleaner, being less influenced by anthropogenic pollution [58]. Also, wind direction was partly dominated by easterly winds, as air masses were transported from Russia and propagated through Belarus before reaching Vilnius. These continental air masses could indicate the significant impact of our neighboring

countries, especially regarding intensive industrial emissions, various combustion processes, and agriculture [59]. Comparing event and non-event cases with backward trajectories, it was suggested that on non-event days, there was a reduced chance of air masses originating from the Baltic Sea direction. This may indicate that air masses originating from the Baltic Sea tend to be cleaner, while those from the continent may be influenced by different kind of pollution or biogenic emissions, potentially with larger particles, and those air masses from the Baltic sea could influence NPF more. According to Bousiotis et al. [55], a long-term study at 13 sites across different European environments found that the trend of cleaner air masses exhibiting a greater probability of NPF events, remained consistent across all examined sites. Studies suggest that continental air typically has larger modal diameters and a greater number concentration [60], which is consistent with this work findings. Thus, important directions to consider that could influence aerosol size distribution when analyzing NPF included the west-north marine and the continental east.

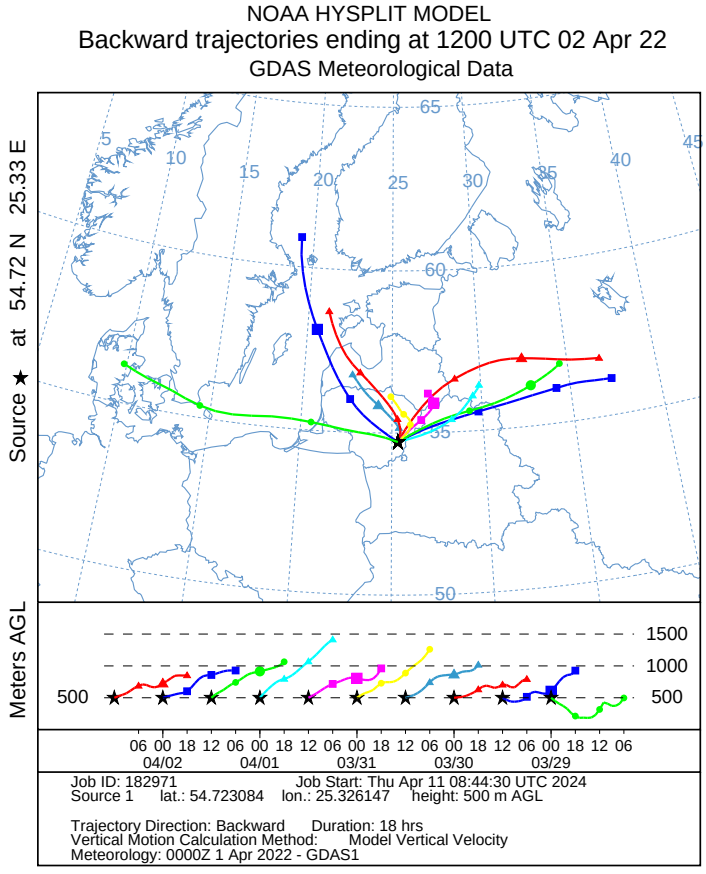

Fig. 4 Backward trajectory analysis for case study of NPF events from March 29 to April 2, 2022 in Vilnius generated by NOAA HYSPLIT model.

3.1.4 Meteorological factors influencing aerosol particle formation

To investigate the relationship between formation episodes and humidity, the most commonly used linear (Pearson) and rank (Spearman) correlation analyses were performed on NPF event days [43]. Pearson's correlation showed a weaker relationship between the variables (mean r = -0.40), while Spearman's correlation revealed a moderate negative correlation (ρ_S = -0.48) (Table

3). A positive correlation was found between nucleation mode concentration and temperature (equal Pearson and Spearman coefficients, ρ = 0.35), but it was weaker than that with relative humidity. No clear correlation was observed between other meteorological parameters, with calculated correlation coefficients close to zero.

To assess potential errors in these correlation coefficients, the bootstrap method was used. From the available sample of 95 values, 1000 new samples were formed, creating new random configurations from resampled correlation coefficient values. These synthetic samples allowed for a more reliable estimation of the 25th and 75th percentile values. The aim of this analysis is to determine the range of correlation values where 50% of the correlation values are statistically likely to be found. Most of the correlation values for wind speed and direction were distributed around zero (Table 3). For relative humidity and nucleation mode, the Pearson coefficient median obtained was r = -0.35. The corresponding 25th and 75th percentile values were -0.66 and -0.13. Similarly, the Spearman median, 25th, and 75th percentile values were -0.54, -0.74, and -0.36, respectively. From the distribution of obtained correlation values, it can be understood that at least half of the correlation values obtained in this way clearly indicated a negative correlation between nucleation mode concentration and relative humidity. Thus, these correlation coefficients indicate that aerosol particle formation was negatively influenced by relative humidity and positively influenced by temperature meteorological parameters.

Table 3 The Pearson and Spearman correlation of nucleation mode and meteorological parameters. Median, 25th and 75th percentiles were calculated using the bootstrap method.

	Pearson correlation				Spearman's rank correlation			
	Mean	Median	25% percentile	75% percentile	Mean	Median	25% percentile	75% percentile
Relative humidity	-0.4	-0.35	-0.66	-0.13	-0.48	-0.54	-0.74	-0.36
Air temperature	0.35	0.35	0.14	0.7	0.35	0.46	0.22	0.69
Wind speed	0.04	0.04	-0.34	0.45	-0.01	0.1	-0.41	0.4
Wind direction	0.02	0.01	-0.26	0.31	-0.01	0.04	-0.4	0.33

Additionally, a comparison of the average relative humidity for event days (RH = 70%) and non-event days (RH = 80%) revealed a clear tendency for relative humidity to be lower during event days. Several reasons have been proposed to explain this strong correlation between ambient relative humidity and the occurrence of NPF. These include the generally negative feedback that high relative humidity exerts on the intensity of solar radiation, photochemical processes, and the atmospheric lifetime of aerosol precursor vapors [53]. Temperature during event days tended to be higher compared to non-event days. While the average ambient temperature on event days was 10.1 ºC, it was lower on non-event days (7.5 ºC). However, this difference was not considered significant

and could be more associated with seasonality [53]. It is known that air masses coming from different directions are influenced by varying levels of biogenic emissions, anthropogenic pollutants, and different weather conditions [53]. Therefore, it is not surprising that there were differences in wind direction between NPF event and non-event days. During event days, the median wind direction was 232º (south-west), whereas during non-event days, it was 156º (south-east). This suggests that air masses traveling from the south-west direction had a higher probability of influencing NPF.

Meteorological factors could correlate not only with NPF event or non-event days, but also with NPF growth rate. In Fig. 5, it is noticeable that there was no strong correlation between growth rate and temperature. However, a correlation with relative humidity showed that increasing relative humidity increased particle growth, indicating that higher humidity leads to faster aerosol particle nucleation and condensation. Regarding wind direction, there were no clear correlation, except for the observation that there was more NPF when the wind prevails from the western direction, as stated before.

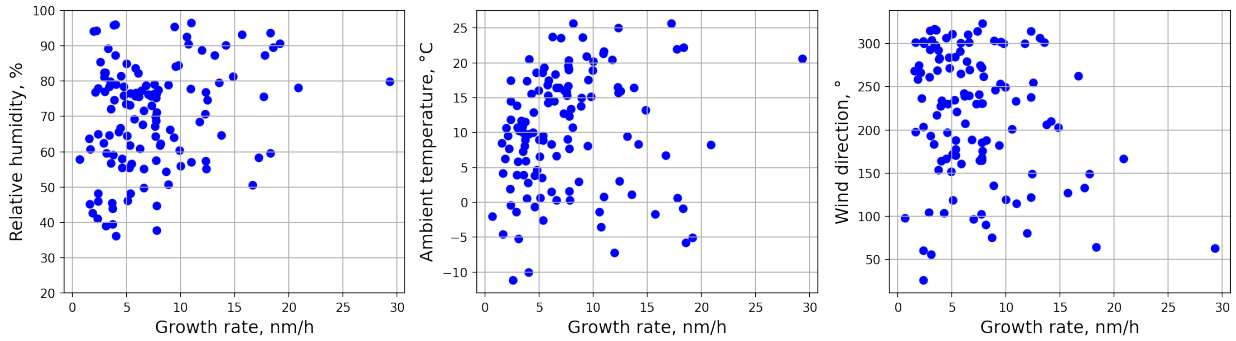

Fig. 5 Relative humidity, ambient temperature and wind direction correlation with NPF growth rate from March, 2022 to February, 2023 in Vilnius, Lithuania.

3.1.5 Aerosol particle number concentration

It has been found that at the Vilnius urban background air pollution Research Station, the average annual aerosol particle number concentration value reached 4560 cm^{-3} (SD = 3020 cm^{-3}). This indicates that the overall particle concentration annual average in the background environment of Vilnius was lower than in other European cities [40, 50, 61], but similar to those found in relatively clean environments [42] and the air of Helsinki [62].

The lowest aerosol particle concentration average was observed in winter, while the highest was in spring. Evaluating the monthly mean values, the lowest concentration was found in January (3310 cm^{-3}), and the highest in March (6120 cm^{-3}) (Fig. 6). The bar chart (Fig. 7) shows the contributions of each mode (nucleation, Aitken, and accumulation) to the total particle concentration. The largest mode contribution to the total particle concentration was observed in the Aitken mode range, ranging from 44% (autumn-winter) to 57% (spring-summer). The highest monthly concentration of this mode (3000 cm^{-3}) was recorded from March to May, while the lowest (1500 cm^{-3}) was in November-January (Fig. 7). Direct traffic flow has a significant impact on the monitoring station for urban background pollution levels. The average diameter of particles emitted by gasoline engines ranges from 40 to 80 nm [63], which may explain the dominance of Aitken mode particles

compared to other modes in urban environments. In contrast, the lowest accumulation mode contribution (18%) was observed in the spring season, while in other seasons it was higher 23-31%, with an annual average particle number concentration of 1190 (SD = 867) cm^{-3}. The highest nucleation mode values were observed in March, April, and October (1460 cm^{-3}, 30% of the total concentration), with an annual average mode of 1200 (SD = 1010) cm^{-3}. The increase in nucleation mode concentration was due to the frequency of new particle formation events observed during these months.

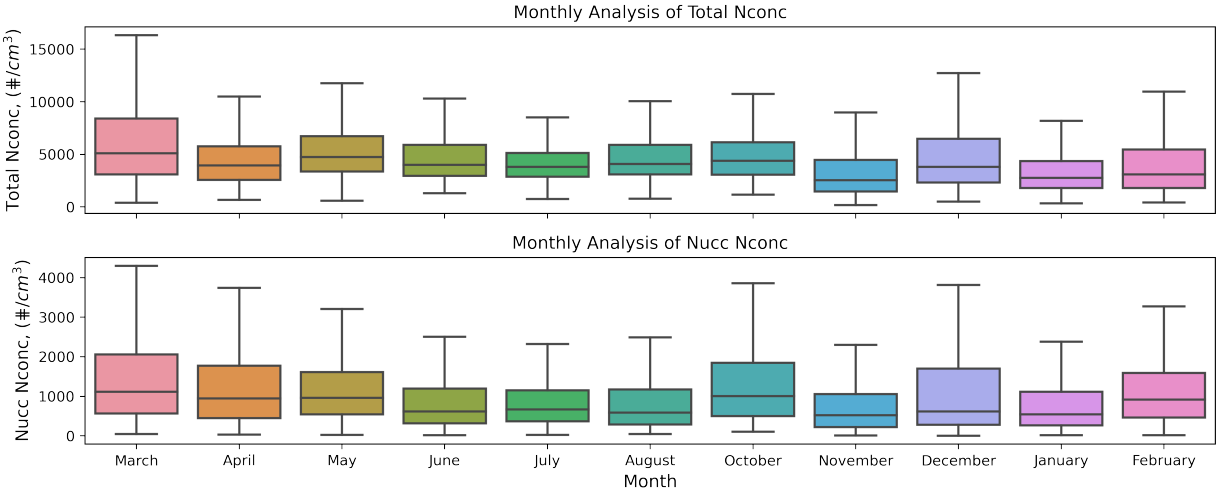

Fig. 6 Monthly aerosol number concentration (total and nucleation (Nucc) modes) measured with the SMPS in Vilnius, Lithuania, during the study period (March 2022 - February 2023). Boxes represent the interquartile range (IQR) between the first (Q1) and third (Q3) quartiles, with the median (50th percentile) indicated by the central line within the box. Whiskers extend to 1.5 times the IQR, encapsulating the majority of the data.

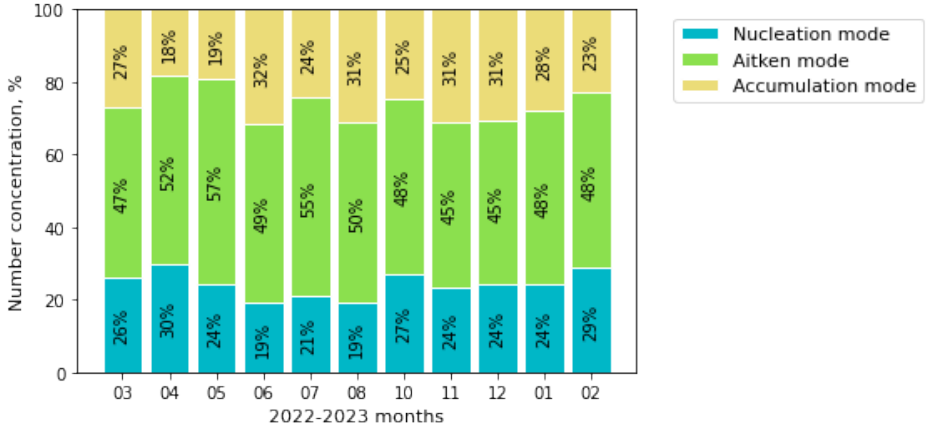

Fig. 7 Monthly contributions of aerosol modes to total aerosol particle number concentration during study period (March 2022 - February 2023) in Vilnius, Lithuania

3.2 Hyltemossa, Sweden

Accurate and reliable measurements of aerosol properties are crucial for understanding their impacts on the environment and human health. One established approach for assessing the consistency and reliability of aerosol measurement data is through closure studies. Closure studies involve comparing data obtained from different instruments or measurement techniques for specific aerosol properties, with the aim of determining if the measurements from a set of instruments align with each other. First part of this chapter is dedicated to comparison of various aerosol measurement instruments for critical aerosol properties, such as mass and number concentration, using data from Hyltemossa Research Station, Sweden. In the second part of this chapter, the aim is to provide insights into new particle formation and submicrometer particles seasonal behaviour.

3.2.1 Closure studies

- CCNC vs MPSS

  Since the MPSS is constructed to count particles, it was decided to compare number concentration measured by MPSS and CCNC. Fig. 8 illustrates the temporal variations in total number concentrations as measured by the Cloud Condensation Nuclei Counter with maximum supersaturation and the Mobility Particle Size Spectrometer over the course of one year. CCNC exhibited less fluctuation compared to MPSS, with an average number concentration of 1209 (SD=729) cm^{-3}, while MPSS average number concentration was 2278 (SD=1964) cm^{-3}. Both instruments showed a noticeable decrease in number concentrations during the winter months (November to February), dropping to 819-902 cm^{-3} in case of CCNC and 1068-1291 cm^{-3} in case of MPSS (Table 4). Notable differences between May - September and October - April aerosol number concentration (SD decreased by 70%) suggested potential variations in measurement techniques or instrument responses.

  When subtracting particles in the smallest size range (5-10nm) from the total number concentration (N(without 5-10nm)) in MPSS, the time series of number concentration showed a similar trend to N(total), with no significant decrease observed. However, subtracting particles in the broader size range of 5-30 nm resulted in a more consistent correlation between CCNC and MPSS, particularly during spring and summer. This implied that fluctuations in these seasons might be attributed to new particle formation, leading to an increase in concentration in the 5-30 nm range. However, excluding particles in the 5-30 nm range showed lower concentration variation compared to CCNC, suggesting that too much data was removed. Hence, the subtraction should be considered somewhere between 5-10 and 5-30 nm.

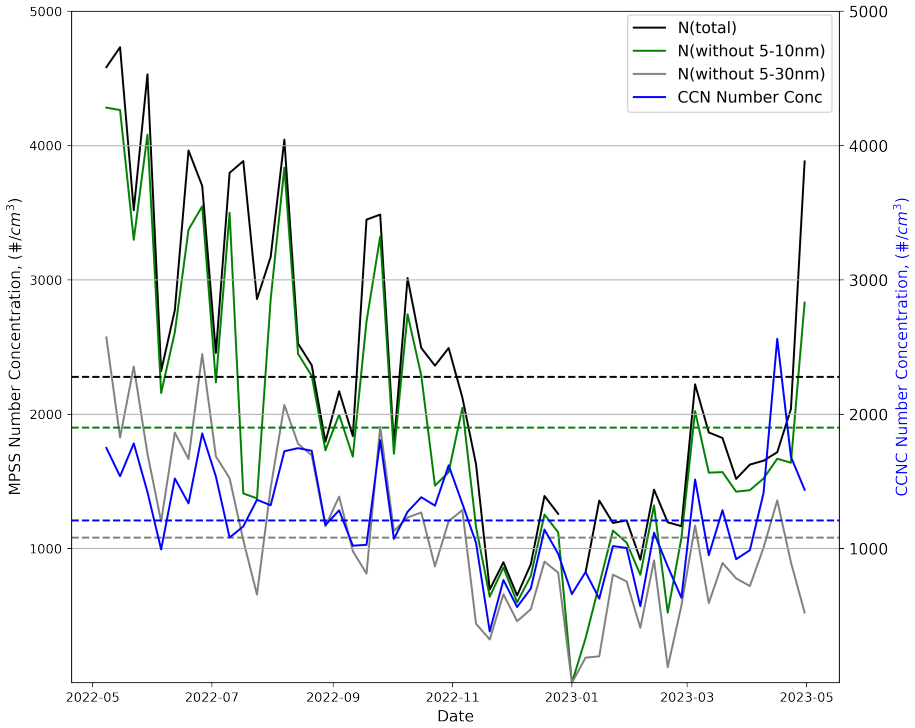

Fig. 8 A time series of CCNC and MPSS weekly number concentrations is presented from May, 2022 to April, 2023 (Hyltemossa, Sweden). The CCNC values are provided at maximum supersaturation (SS), while MPSS concentrations are divided into size ranges: total, total excluding the 5-10 nm size range, and total excluding the 5-30 nm size range. Dotted lines represent annually average concentrations.

Table 4 Seasonal statistics of number concentration, including mean, standard deviation (SD), median (50%) monthly averaged values. Concentrations are provided for total number concentration (measured by MPSS), nucleation (Nucc) mode (5-30 nm size range) number concentration (measured by MPSS) and number concentration at maximum SS (measured by CCNC).

	N_{total} (MPSS)			N_{Nucc} (MPSS)			N_{total} (CCNC)		
Month	mean	SD	50%	mean	SD	50%	mean	SD	50%
May	4124	3083	3231	2114	3338	847	1661	857	1467
June	3174	2000	2727	1261	1775	648	1478	705	1344
July	3308	2288	2637	1234	2119	416	1251	726	1129
August	2614	1837	2059	941	1505	431	1561	647	1455
September	2617	2104	2075	1316	1982	612	1245	602	1144
October	2520	1279	2290	970	1320	572	1371	708	1231
November	1291	925	978	640	3287	280	842	554	717
December	1068	740	774	248	495	122	834	536	659
January	1143	915	982	406	1395	237	819	574	664
February	1286	857	1061	560	723	392	902	729	648
March	1810	1073	1584	1011	1207	649	1112	807	829
April	2220	1934	1740	1249	2361	398	1592	712	1511

Forces between molecules at the surface change with aerosol curvature. For small particles, there are fewer forces between (water) molecules, making it harder to keep/attract-bond water, and more likely to evaporate than to condensate and grow. This phenomenon, known as the Kelvin or curvature effect, increases with decreasing particle sizes [13]. It could explain why CCNC may not activate smaller particles even with supersaturation greater than 1, due to the curvature of the particles. The closure was reasonable because CCNC's total concentration should be lower compared to MPSS concentration, accounting for the smaller particles counted only in MPSS (Fig. 9).

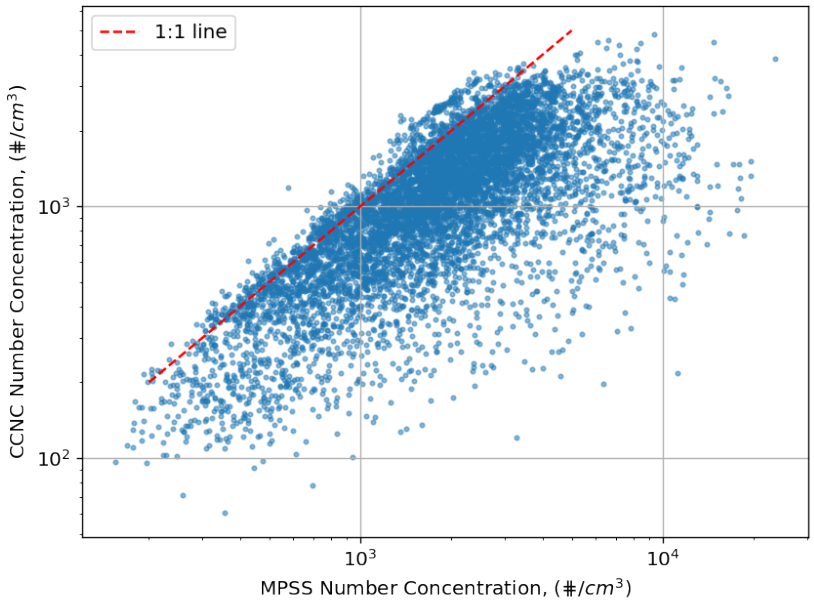

Fig. 9 A scatterplot comparing concentration of CCNC (with maximum SS) to the total number concentration measured by MPSS from May, 2022 to April, 2023 (Hyltemossa, Sweden)

- FIDAS vs MPSS

  The time series analysis of FIDAS mass concentration in comparison to MPSS volume concentration revealed important correlation. The FIDAS mass concentration was higher than the MPSS volume concentration (Fig. 10). It was logical considering that mass concentration and volume concentration is not the same measure and varies through density multiplication. Notably, the discrepancy between the two instruments became more evident from around October. This temporal evolution suggested a potential issue with one or both instruments during cold period.

  Examining the ratio of PM1 mass concentration (FIDAS) to volume concentration (MPSS) provided insights into the density of aerosol particles (Fig. 11). The density fluctuated between 2 and 3 $\mu g/cm^3$ from October 2022 to May 2023, while during the spring and summer of 2022, it remained lower, ranging from 1 to 2 $\mu g/cm^3$. The expected density varies between 1-2 $\mu g/cm^3$ [64, 65], implying a deviation from the norm starting in October. This anomaly

raised concerns about the reliability of either the FIDAS or MPSS instrument during this time frame. Also, this variation could indicate something noteworthy about MPSS volume concentration due to similar increasing pattern in number concentration fraction between CCNC and MPSS.

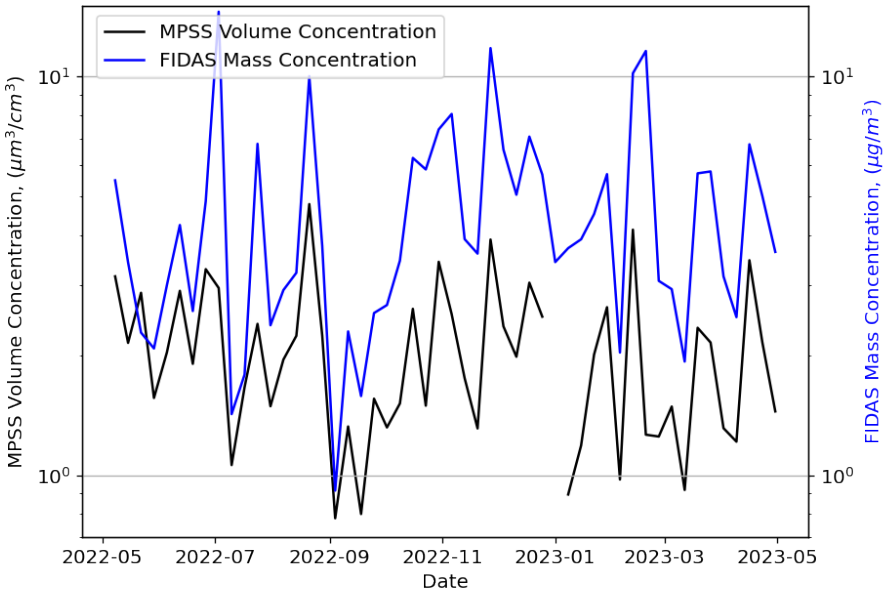

Fig. 10 Time series of FIDAS PM1 concentration and MPSS volume concentration (weekly averages) from May, 2022 to April, 2023 (Hyltemossa, Sweden).

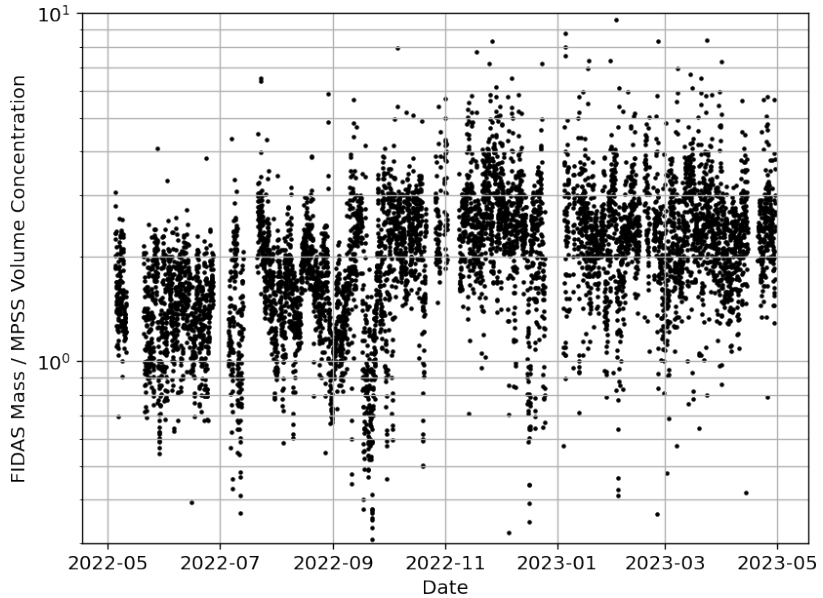

Fig. 11 Time series showing the ratio between PM1 (measured by FIDAS) and volume concentration (measured by MPSS) from May, 2022 to April, 2023 (Hyltemossa, Sweden).

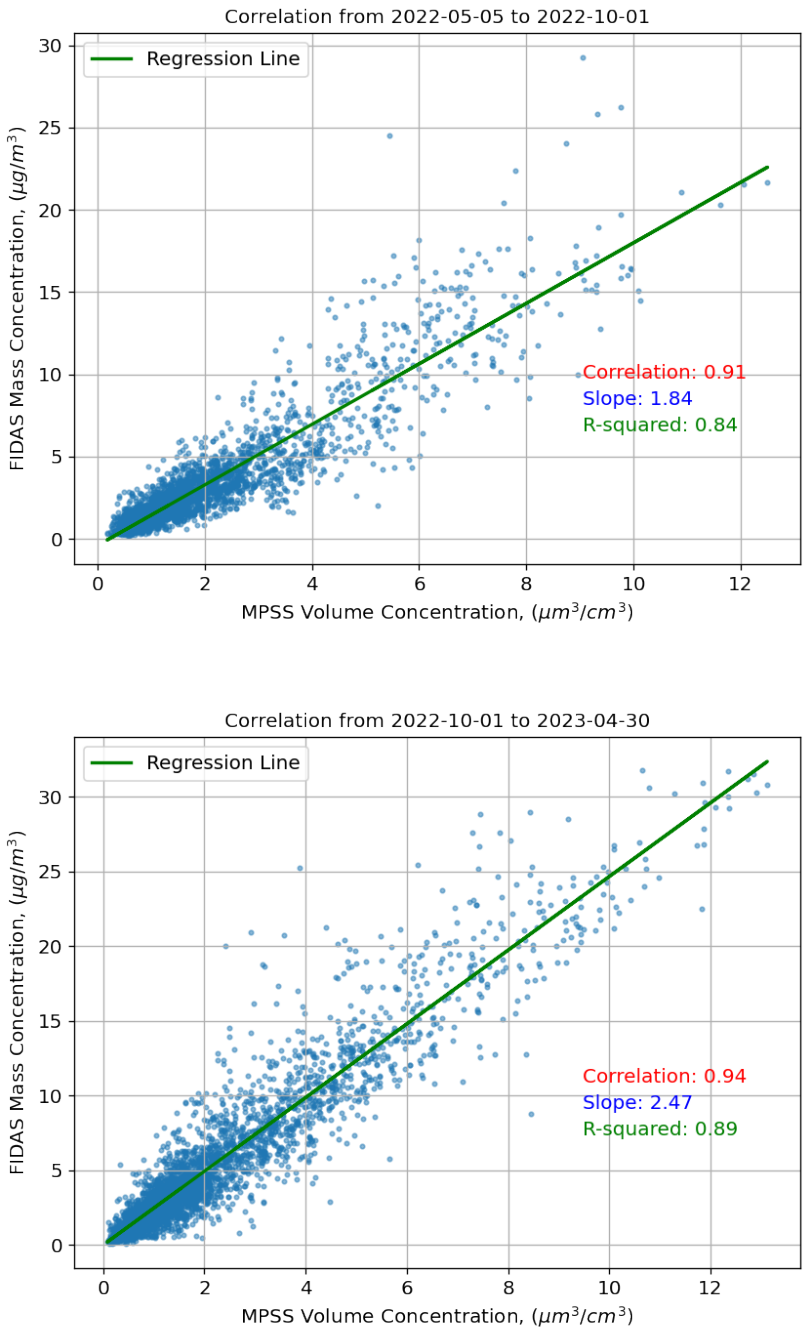

Fig. 12 A scatterplot of FIDAS vs. MPSS, divided into two periods: May 5th to October 1st (up) and October 1st to March 30th (down) (Hyltemossa, Sweden); as well as statistical parameters: correlation coefficient, slope, r-squared value, regression line.

Furthermore, examining the correlation between FIDAS and MPSS, when divided into distinct periods, the slope of the correlation changed (Fig. 12). From May 2022 to October 2022, the slope was 1.84, indicative of a density within normal ranges. However, from October 2022 to April 2023, the slope increased to 2.47, suggesting a noteworthy deviation. This temporal slope shift highlighted the importance of a deeper investigation into the specific time periods to identify potential issues affecting the concentrations recorded by the instruments. Despite this change in slope, the correlation coefficient remained relatively stable, shifting from 0.92

to 0.94, indicating a very strong linear relationship between the instruments. The R-squared coefficient also showed consistency, moving from 0.84 to 0.89. These R-squared values signify that approximately 84% to 89% of the variability in the dependent variable (FIDAS) could be explained by the independent variable (MPSS), reinforcing the robustness of the linear correlation observed between the two datasets.

- ACSM and AE33 vs MPSS

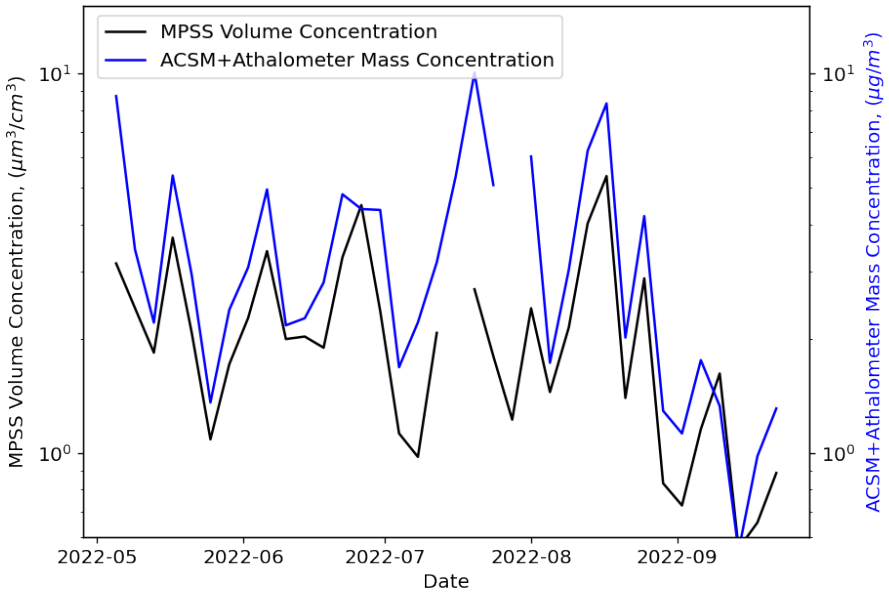

Fig. 13 Time series of PM1 mass concentration measured with ACSM and AE33 and volume concentration measured with MPSS (4-day averages) from May 5 to September 22, 2022 (Hyltemossa, Sweden).

The comparison with ACSM data was constrained by the availability of data until September 22nd (Fig. 13), characterized by frequent short breaks and instrument failures. Noteworthy variations in density, particularly a density increase in early May (Fig. 14), coincided with higher concentrations in NO_3 and organics. The decline in the relative ionization efficiency of NH_4 (RIENH4) from 4.2 to 3.6 by May 9th suggested a potential impact on ammonium concentration (Fig. 15). This parameter indicates how efficient it can ionize aerosol particles. Stable RIENH4 is crucial for accurate monitoring, emphasizing the need for instrument stability. Furhermore, instances of negative or very low concentrations around zero in mid-June, as well as lower concentrations and a fraction of about 0.3 on June 26th and 27th, indicated potential problems, possibly related to calibration or other operational issues. These anomalies necessitate further investigation to identify underlying causes. In mid-September, a drop in ACSM concentration corresponded to a decrease in flow rate ($flow_{ccs}$) to 1.2, below the typical rate of 1.4 (Fig. 16). This divergence in flow rate could account for the lower concentration during this period, underlining the importance of maintaining optimal operational parameters.

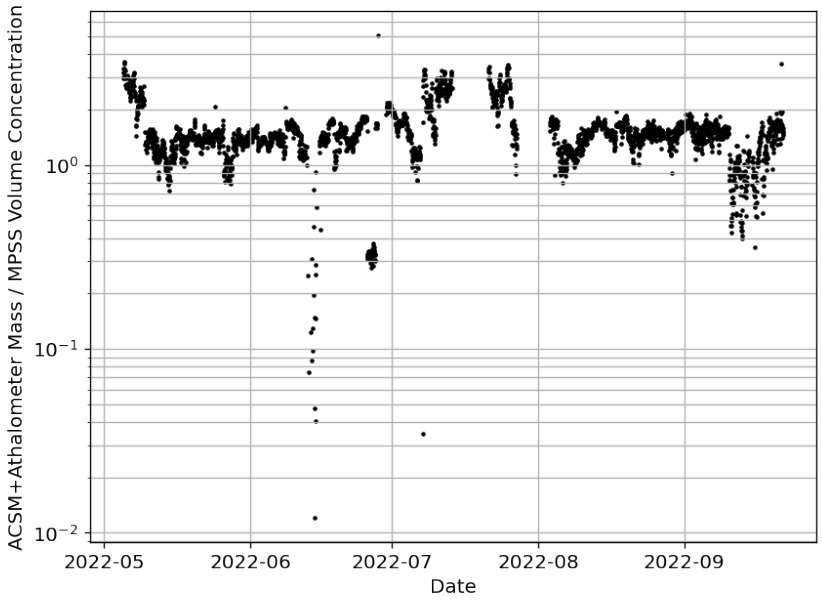

Fig. 14 Time series showing the ratio between PM1 (measured by ACSM and AE33) and volume concentration (measured by MPSS) from May 5 to September 22, 2022 (Hyltemossa, Sweden)

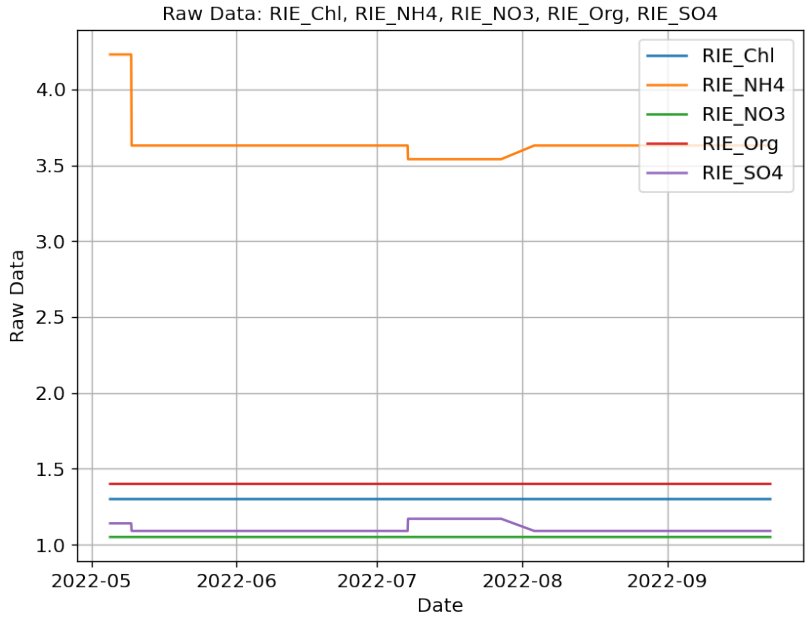

Fig. 15 Time series of ACSM parameters: relative ionization efficiency (RIE) of Chl, NH4, NO3, Organic, SO4, measured from May 5 to September 22, 2022 (Hyltemossa, Sweden).

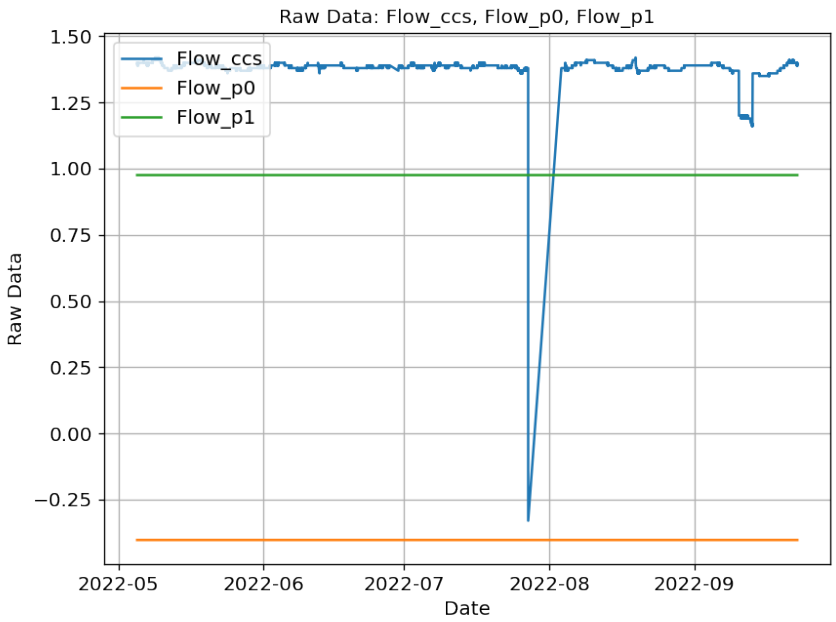

Fig. 16 Time series of ACSM flow rate and pressure parameters, measured from May 5 to September 22, 2022 (Hyltemossa, Sweden).

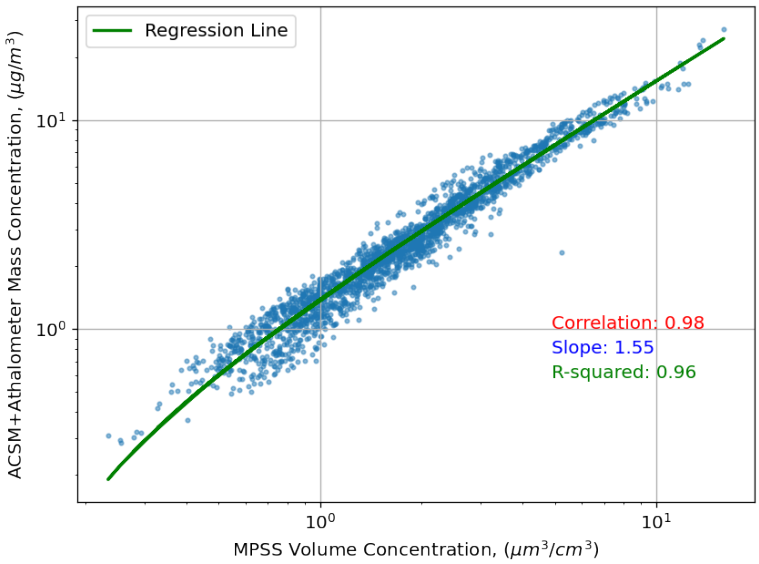

Fig. 17 A scatterplot comparing mass concentration of ACSM and AE33 to volume concentration measured by MPSS as well as statistical parameters: correlation coefficient, slope, r-squared value, regression line (Hyltemossa, Sweden).

Despite these challenges, the average fraction of PM1/Volume concentration maintained a typical value of 1.496 $\mu g/cm^3$, suggesting reasonable agreement between ACSM and MPSS instrument data (Fig. 17). After data cleaning and correlation analysis, the slope became 1.55, indicating logical results for aerosol particle density to be equal to 1.55 $\mu g/cm^3$. High

correlation (r = 0.98) and r-squared parameters (R^2 = 0.96) further supported a commendable agreement between the datasets, underscoring the importance of addressing discrepancies to enhance the reliability of aerosol measurements.

- ACSM and AE33 vs FIDAS

  The comparison of time series data for mass concentration among ACSM and AE33 and FIDAS instruments reveals a generally agreeable pattern (Fig. 18) - FIDAS PM1 concentration and ACSM and AE33 PM1 concentration shows similar tendency of time series. This similarity extended to the comparison with MPSS volume concentration, suggesting that many of the observed fluctuations could be attributed to common factors affecting ACSM. Notably, discrepancies in the ups and downs coincided with ACSM flow rate or relative ionization efficiency issues, as indicated in Fig. 19. However, the ratio data exhibited more pronounced fluctuations, with an average value of 1.1254, deviating from the expected value of around 1 as there was the same mass concentration measure but it could be different size range for measuring.

  Upon cleaning the ACSM data to address these discrepancies, the slope of the correlation is reduced to 0.82 (Fig. 20), indicating a slightly lower value than expected (expected value around 1, since it is the same measure - mass concentration PM1). Nevertheless, the correlation coefficient remains at 0.87, and the R-squared parameter at 0.75, signifying a reasonably good correlation between the datasets. These results underscore the importance of meticulous data cleaning and the potential need for further investigation into the factors influencing the observed fluctuations in the mass concentration data.

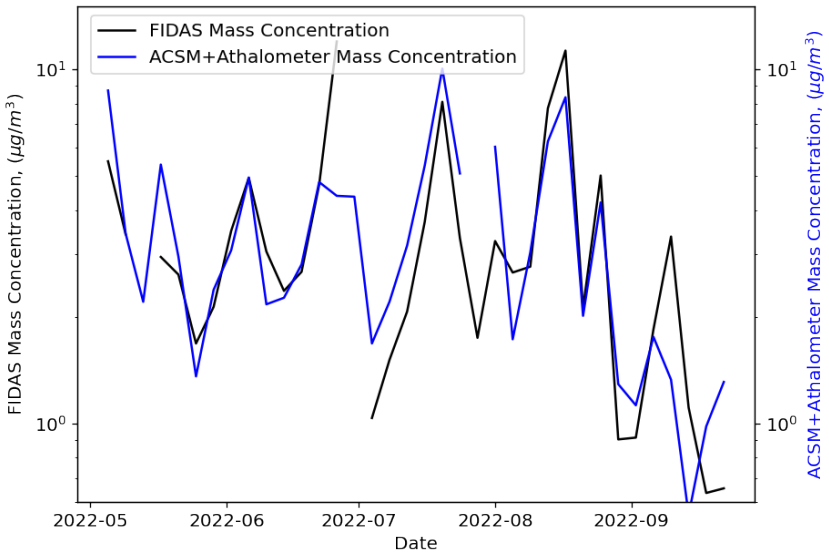

Fig. 18 Time series of FIDAS PM1 concentration and ACSM and AE33 PM1 concentration (4-days averages), measured from May 5 to September 22, 2022 (Hyltemossa, Sweden).

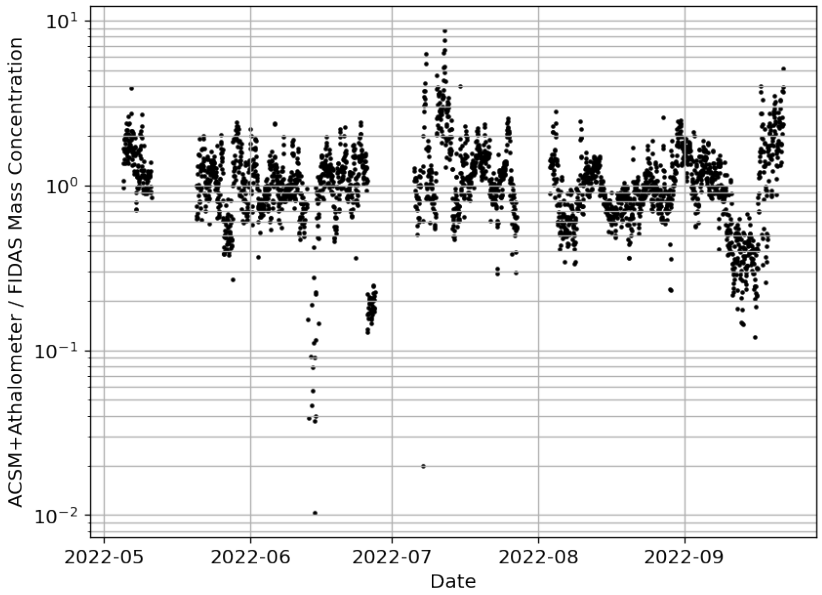

Fig. 19 Time series showing the ratio between mass concentration (measured by ACSM and AE33) and PM1 mass concentration (measured by FIDAS), measured from May 5 to September 22, 2022 (Hyltemossa, Sweden)

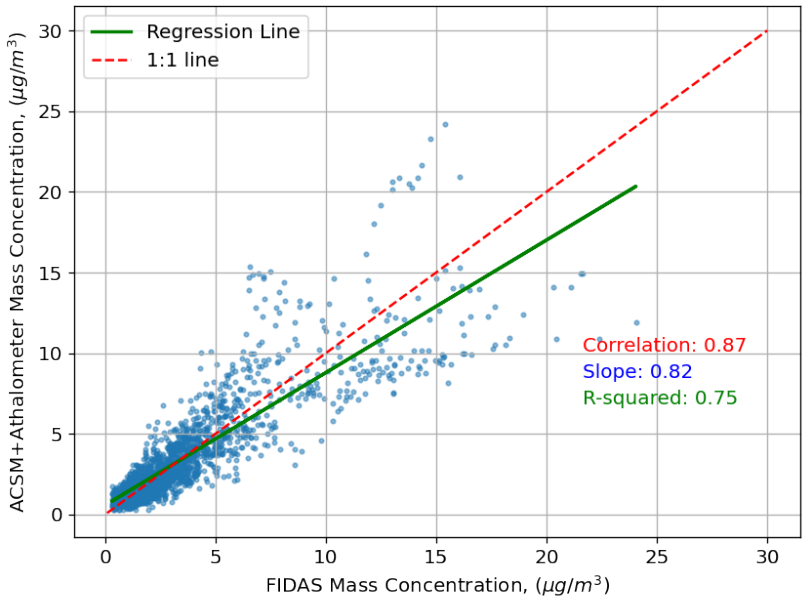

Fig. 20 A scatterplot comparing mass concentration of ACSM and AE33 to PM1 measured by FIDAS as well as statistical parameters: correlation coefficient, slope, r-squared value, regression and 1:1 line (Hyltemossa, Sweden).

- Mass concentration of MPSS

In earlier sections, the MPSS instrument was primarily evaluated based on its number concentration or volume concentration. However, it was feasible to compute the mass concentration of MPSS

data by using ACSM and AE33 data for density calculations and multiplying MPSS volume by the obtained density (see formula 2). Fig. 21 presents the PM1 mass concentrations from FIDAS and ACSM, AE33, in comparison with MPSS mass concentration. The comparison highlighted a robust closure between these instruments. The correlation of MPSS mass concentration with ACSM and AE33 data was notably stronger, as the density was derived from this dataset, yielding a slope of 1.13 and a correlation coefficient of 0.97, this indicated a very strong positive linear relationship between the two datasets. ACSM and AE33 data had a high R-squared value of 0.94, indicating that 94% of the variability in the mass concentration can be explained by the variability in these datasets. Nevertheless, the correlation with FIDAS was also very good but slightly weaker, featuring a slope of 1.32 and a correlation coefficient of 0.92 and 84% of the variability in the mass concentration could be explained by the variability in the FIDAS dataset. Compared to Fig. 12 and Fig. 17 correlation values found similar. These findings underscored the reliability and consistency in mass concentration measurements across the evaluated instruments, further supporting the comprehensive assessment of aerosol characteristics in this study.

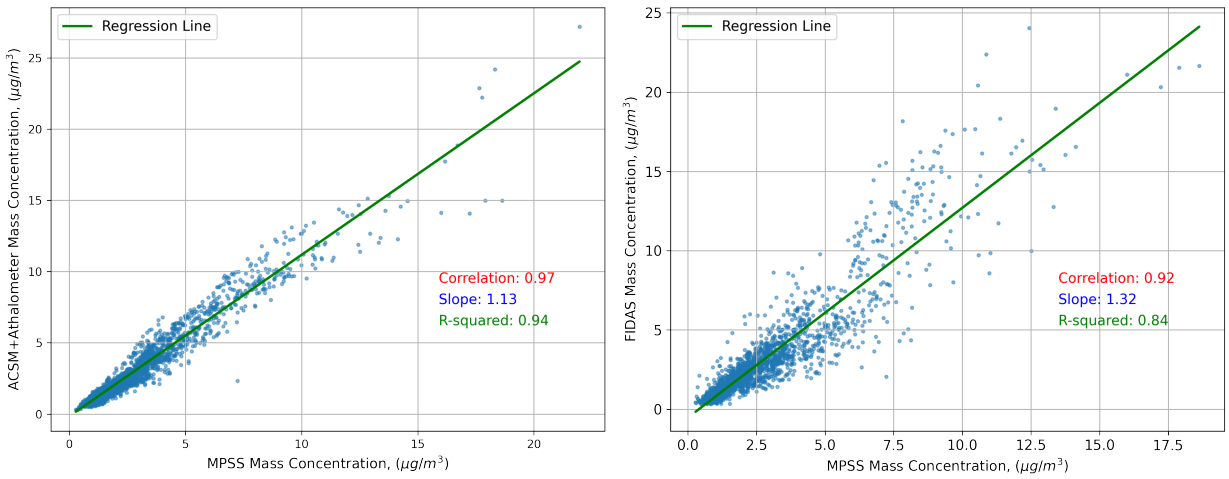

Fig. 21 A scatterplot comparing the mass concentration of ACSM and AE33 to the mass concentration calculated from MPSS (left), and PM1 concentration measured with FIDAS to the mass concentration calculated from MPSS (right); as well as statistical parameters: correlation coefficient, slope, r-squared value, regression line (Hyltemossa, Sweden).

3.2.2 Seasonal behavior of aerosol concentration

The lowest average number concentration of aerosol particles was observed in winter, and the highest was observed in spring. When evaluating monthly average values, the lowest concentration was found in January (774 cm^{-3}), and the highest was found in May (3231 cm^{-3}) (Fig. 22). In May, 50% of the number concentration was in the Nucleation mode (5-30 nm), indicating that the highest concentration during this month was due to the formation of new particles. Additionally, the highest variation in May and July could also be explained by new particle formation during the warm season. The CCNC number concentration followed a very similar pattern to the MPSS number concentration, with the highest concentration in the warm season and the lowest concentration in the cold season. However, it could be noted that the CCNC number concentration stays higher

for longer periods from mid-spring to mid-autumn, while the MPSS number concentration peaked in spring and the beginning or mid-summer. This could also be explained by how these different instruments manage to measure concentration, as the CCNC could not measure the nucleation mode that significantly influences MPSS concentration during specific periods [53, 66]. Total average concentration for MPPS was found 2278 cm^{-3} (Table 5), indicating similar results as in other rural or forest areas [67].

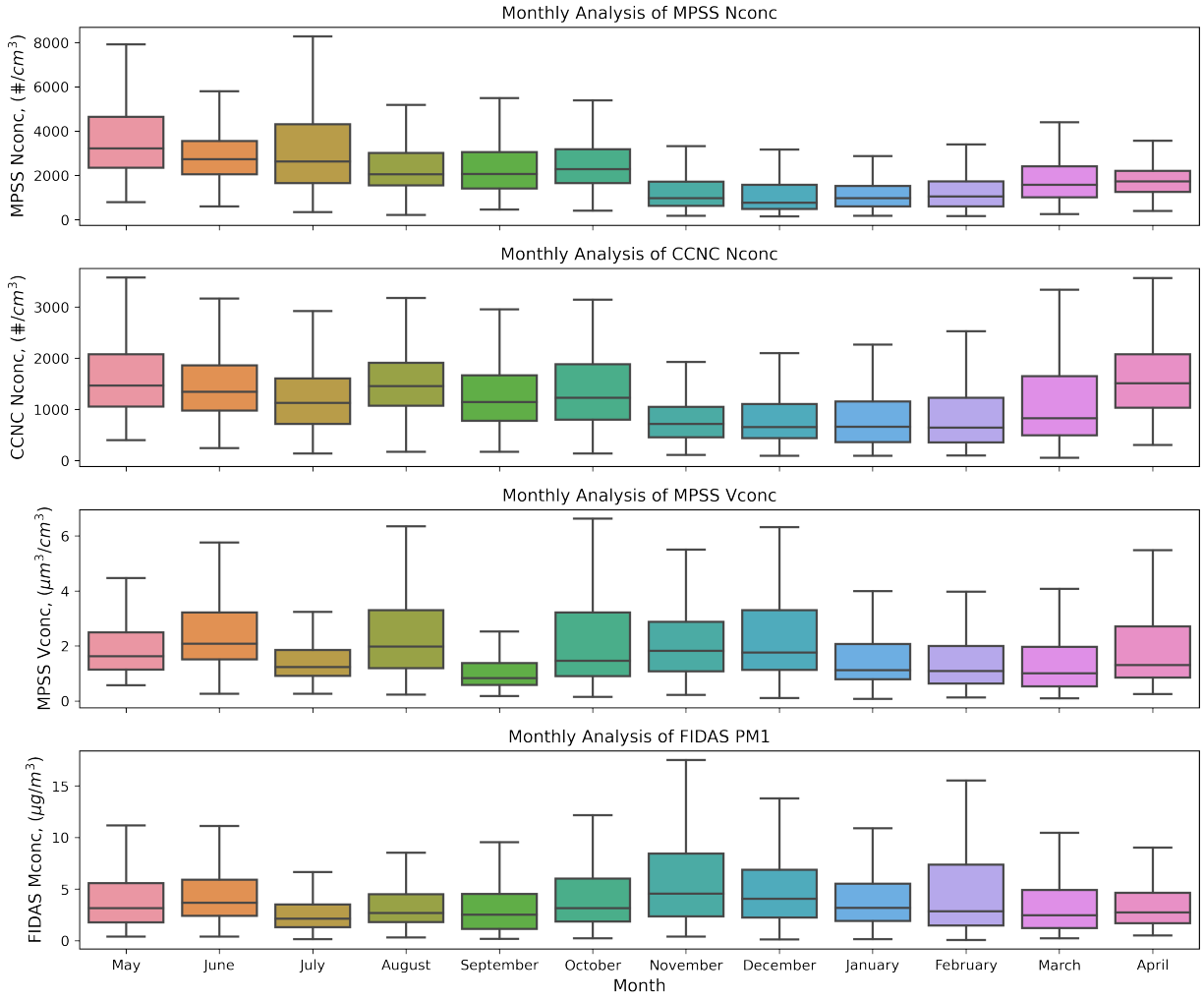

Fig. 22 Monthly aerosol concentration measured with MPSS (number and volume concentration), CCNC (maximum SS) and FIDAS (PM1 mass concentration) from May, 2022 to April, 2023 (Hyltemossa, Sweden). Boxes represent the interquartile range (IQR) between the first (Q1) and third (Q3) quartiles, with the median (50th percentile) indicated by the central line within the box. Whiskers extend to 1.5 times the IQR, encapsulating the majority of the data.

The MPSS volume concentration exhibited an opposite pattern compared to the number concentration. More variations with higher concentrations were observed during the colder period from October to January (median value of 1.8 m^{-3} in November and December). However, in June and August, similarly high concentrations were also observed (median value of 2 m^{-3}). While average concentration peaked in June (2.7 m^{-3}) and December (2.5 m^{-3}). The FIDAS PM1 concentration clearly showed an increase from October to February and a decrease from March to September. The highest average concentration was observed in November (6.9 $\mu g/m^3$) and February (7 $\mu g/m^3$),

while the lowest average concentration was observed in July (3.1 $\mu g/m^3$) (Table 5). This could be explained by the dominance of larger particles during colder seasons, attributed to increased anthropogenic pollution resulting from elevated activities such as cooking, heating, and transportation [68, 69].

PM1 mass concentration measured with ACSM and AE33 had highest average concentration in July (4.6 $\mu g/m^3$), the lowest in September (1.2 $\mu g/m^3$). These values were similar to FIDAS measured PM1 during summer period. Calculated mass concentration from MPSS was slightly lower, with highest average concentration during June (3.8 $\mu g/m^3$) and the lowest (1.3 $\mu g/m^3$) during September similarly as PM1 from ACSM and AE33 (Table 5). PM1 concentrations in this rural area closely aligned with an average concentration of 3.6-5.6 $\mu g/m^3$ found in the literature [70]

Table 5 Seasonal statistics of volume and mass concentration, including mean, standard deviation (SD), median (50%) monthly averaged values. Concentrations are provided for total volume concentration (measured with MPSS), total mass concentration (calculated using MPSS total volume), PM1 mass concentration (measured with FIDAS) and PM1 mass concentration (measured with ACSM and AE33).

	Vconc (MPSS)			Mconc (MPSS)			PM1 (FIDAS)			PM1 (ACSM&AE33)		
Month	mean	SD	50%	mean	SD	50%	mean	SD	50%	mean	SD	50%
May	2.3	2.0	1.6	3.2	2.9	2.3	4.1	3.1	3.2	3.8	4.5	2.4
June	2.7	1.9	2.1	3.8	2.6	3.0	4.8	3.6	3.7	3.5	2.6	2.7
July	1.6	1.3	1.2	2.4	1.9	1.8	3.1	3.1	2.2	4.6	4.9	2.8
August	2.6	2.0	2.0	3.6	2.8	2.8	4.0	3.6	2.7	4.0	3.2	2.9
September	1.2	0.9	0.8	1.3	0.9	1.0	3.7	3.7	2.5	1.2	0.7	1.0
October	2.2	1.8	1.5				4.8	4.6	3.2			
November	2.4	2.0	1.8				6.9	6.6	4.6			
December	2.5	2.0	1.8				5.4	4.6	4.1			
January	1.8	1.7	1.1				4.3	3.9	3.2			
February	2.0	2.6	1.1				7.0	9.3	2.9			
March	1.7	1.9	1.0				4.2	4.7	2.5			
April	2.0	1.7	1.3				3.9	3.3	2.8			

Furthermore, the Conditional Parameter Factor (CPF) analysis was used to identify likelihood of high concentrations occurrences based on wind direction and speed. In Fig 23, there is a CPF polar plot depicting wind direction and speed, as well as number and PM1 mass concentration. It was found that there was a higher chance of having a higher number concentration when the stronger was blowing (more than 6 m/s) from the west or northwest and with slower wind speed from the south. To the west of Hyltemossa station lies Helsingborg, the second-largest city in Scania. Additionally, the Port of Helsingborg is the second-largest container port in Sweden and one of the leading ports in Northern Europe. This could influence an increase in particle number concentration and transport to the land into the forests. Additionally, it was discovered that moderate wind from the south-west and south-east increases the likelihood of having a higher PM1 concentration (measured by FIDAS).

In the south-west direction, CPF could be influenced by city pollution from places like Lund and Malmo. However, the south-west direction is rural in Skania, suggesting the possibility of long-range transport from Eastern or Central Europe. This suggestion is supported by recent research [71], which concluded that the majority of the background black carbon mass concentrations in southern Sweden originate from continental Europe.

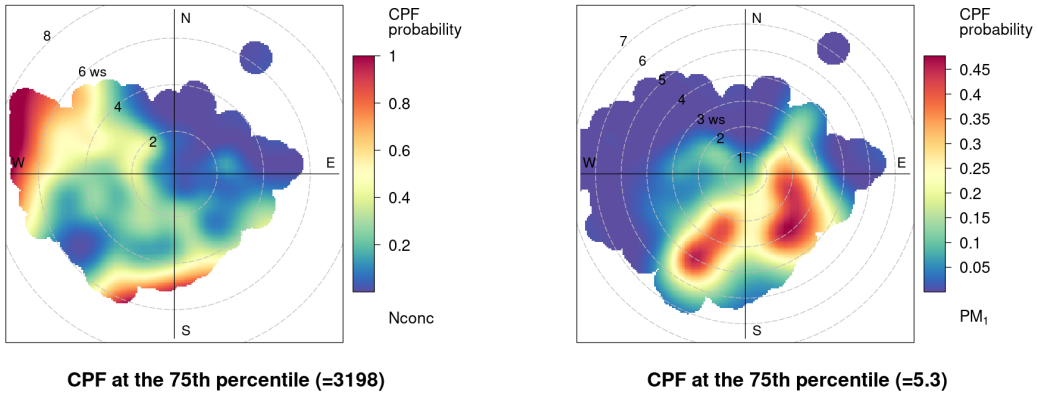

Fig. 23 Conditional Probability Functions (CPF) for MPSS total number concentration (left) and PM1 mass concentration from FIDAS (right) (from May, 2022 to April, 2023, Hyltemossa, Sweden). On the left, the CPF depicts the probability distribution of MPSS total number concentrations based on varying combinations of wind speed (in m/s) and direction (in degrees). The vertical color bar represents the probability of an MPSS total number concentration, while the polar plot displays wind speed and direction alongside the CPF. The CPF on the right performs a similar analysis for PM1 mass concentration measured by FIDAS.

3.2.3 New particle formation events

For further analysis of MPSS data, it was chosen to analyze new particle formation events on a day-by-day basis. A total of 337 days were analyzed. By examining the percentage variation, Fig. 24 illustrates how NPF frequency varied throughout the year. NPF peaked during July, reaching 79%. Notably, during the spring months and June, July event days constituted 60% or more. This study revealed that the lowest NPF frequency occurred in November (30%), December (40%), and January (30%). When compared to another Swedish measurement station [72], NPF frequency showed considerable similarity during the peak of NPF in summer months (more than 70% NPF events in June and around 50% NPF events in July, August). However, during other months in this study, there was 40% or less NPF frequency. It should be noted that this location is significantly farther north, which could imply different meteorological conditions for NPF occurrence.

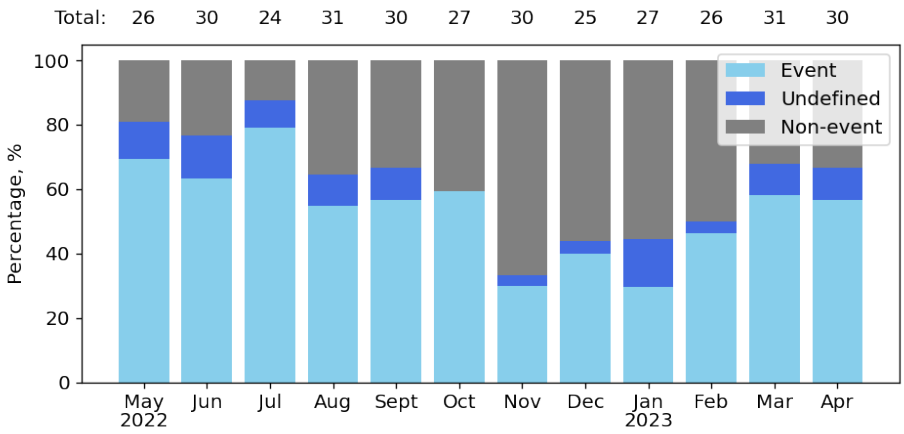

Fig. 24 Frequency of new particle formation event occurrence from May, 2022 to April, 2023 (Hyltemossa, Sweden).

In this study, the majority of events occurred during the daytime, as shown in Fig. 25, where the growth rate of NPF event days is plotted as a function of NPF onset time. The overall growth rates consistently stayed below 10 nm/h, with occasional outliers. Events happening at nighttime seemed to exhibit higher growth rates, with a maximum of 22 nm/h during the autumn season. Moreover, the median growth rate was higher during winter (5.7 nm/h), while in other seasons, the median stayed between 2.5 to 4.2 nm/h. This was also applicable to monthly averaged data, when mean growth rate peaks in December (9.2 nm/h) (Fig. 26). This implied that during colder seasons, there was fewer NPF events, and they occurred more rapidly (with higher growth rate). In comparison with [72], who reported growth rate in the range of 0.5 to 10 nm/h during daytime and over 10 nm/h at nighttime events, the GR showed similar values, but at Hyltemossa Station, fewer events occurred during nighttime. In the article [53], growth rate statistics are provided based on site type classification in the literature. Their classification placed Hyltemossa Station in the categories of remote or rural (Table 3, reported median GR of 3.5 nm/h).

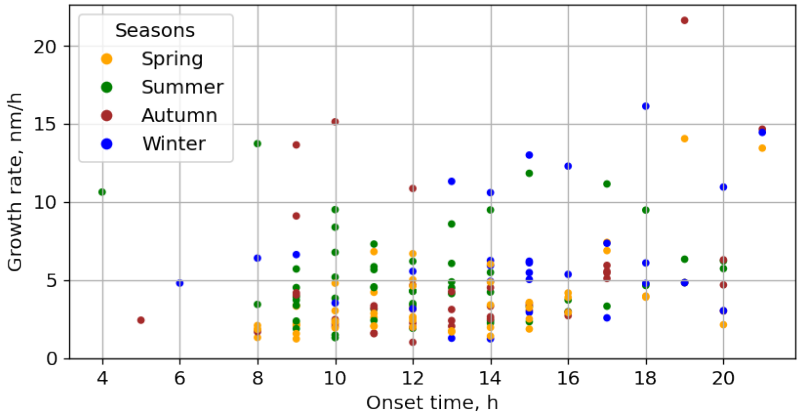

Fig. 25 Growth rate for the events as a function of NPF onset time. The colors indicate different seasons as explained in the legend (Hyltemossa, Sweden).

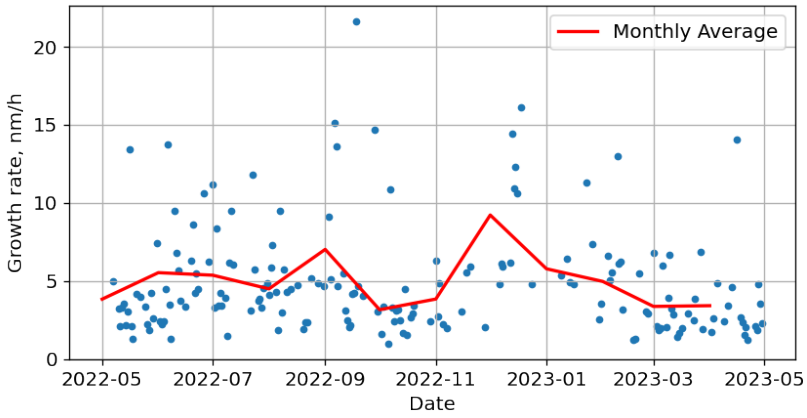

Fig. 26 A scatterplot illustrating daily growth rates alongside a line depicting monthly averages (Hyltemossa, Sweden)

Looking into what meteorological factors influence NPF, the most significant factor influencing whether atmospheric NPF were the amount of solar energy that reaches the Earth's surface [73,74]. In this work, it was found that average net solar radiation (NETRAD) intensity was higher during NPF event days (averaged NETRAD = 83.7 W/m^2) compared with non-event days (averaged NETRAD = 46.7 W/m^2). The incoming short-wave (SW IN) radiation was notably 79% stronger during event days (SW IN = 158.3 W/m^2) compared to non-event days (SW IN = 88.7 W/m^2). Additionally, a strong trend for relative humidity to be lower on event days was seen when comparing the average RH for event days (81.2%) with that of non-event days (90.3%). Temperatures during event days tended to be higher compared to non-event days. While on event days averaged ambient temperature was 9.5 °C, on non-event days it was lower 8.0 °C. However, the difference was not significant, it could be more likely associated with seasonality. Furthermore, the median wind direction on event days was 224 ° (south-west), and it was 153 ° (south-east) on non-event days. This indicates that air masses moving in from a southwesterly direction were more likely to affect NPF. Vice versa, air masses moving in from the southeast were less likely to affect NPF. Those air masses from the southeast direction were associated as major contributors to the background mass concentrations in southern Sweden [71], indicating that polluted air masses arriving from the southeast tended to reduce new particle formation.

Moreover, growth rate correlation with meteorological parameter showed weak or no correlation (Fig. 27). Even though, increasing relative humidity correlated with increasing growth rate, meaning quicker condensation processes.

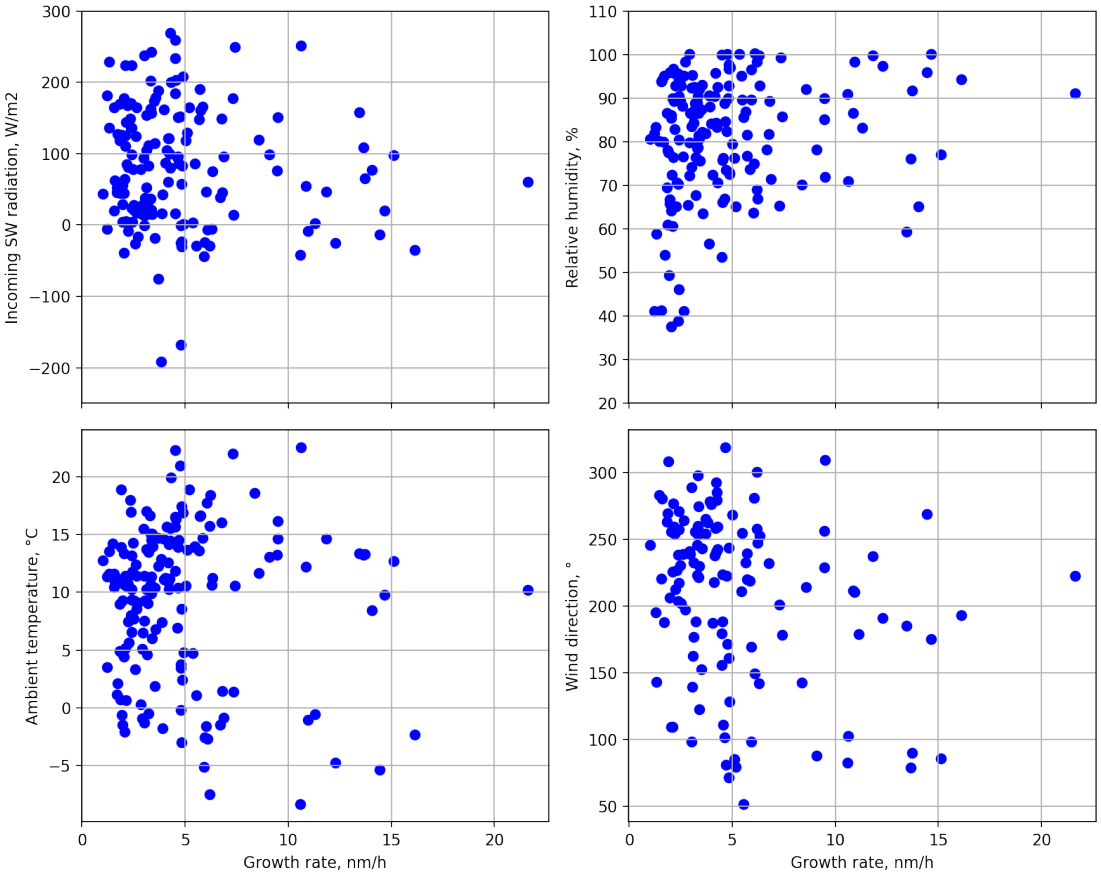

Fig. 27 Correlation of incoming shortwave (SW) radiation, relative humidity, ambient temperature and wind direction with NPF growth rate from May, 2022 to April, 2023 in Hyltemossa, Sweden

3.3 Abisko, Sweden

3.3.1 Quality of AIS-data

By comparing the positive and negative ion values from the AIS-data, there were large differences for particle diameter below 4 nm due to no negative ions in this range being detected (Fig. 28). In addition, the AIS showed higher concentration of negative ions in the 10-20 nm range, seen as a band from end of June and onward in Fig. 28.

However, when comparing the AIS data with SMPS, both instruments managed to capture different size distributions similarly both in space and time in the particle diameter overlap region (9-40 nm). The size distribution and its evolution in time for one of the most obvious NPF events (banana shaped pattern) during the summer of 2023 is shown in Fig. 29, captured both by SMPS and positive ions of the AIS. This suggested that the AIS data was usable when focusing on the positive ions. For future studies and moving forward in this project, the AIS data for positive ions could be used as a complement to the SMPS data.

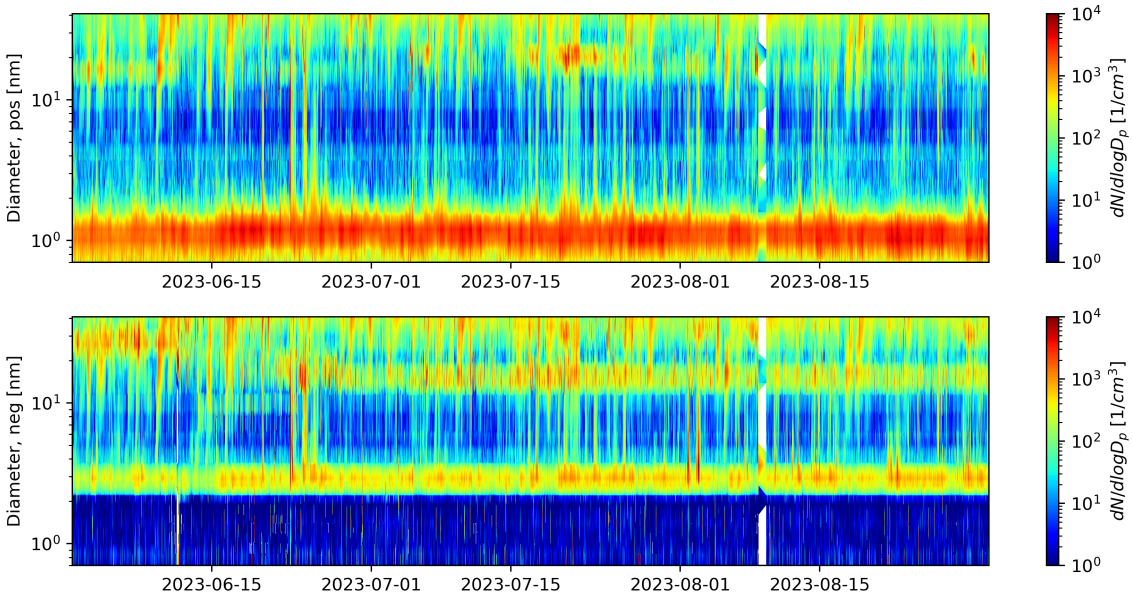

Fig. 28 Particle size distribution for each time step during summer 2023 as measured by AIS. Positive ions on top, negative below. The colormap indicates the number concentration at a given point.

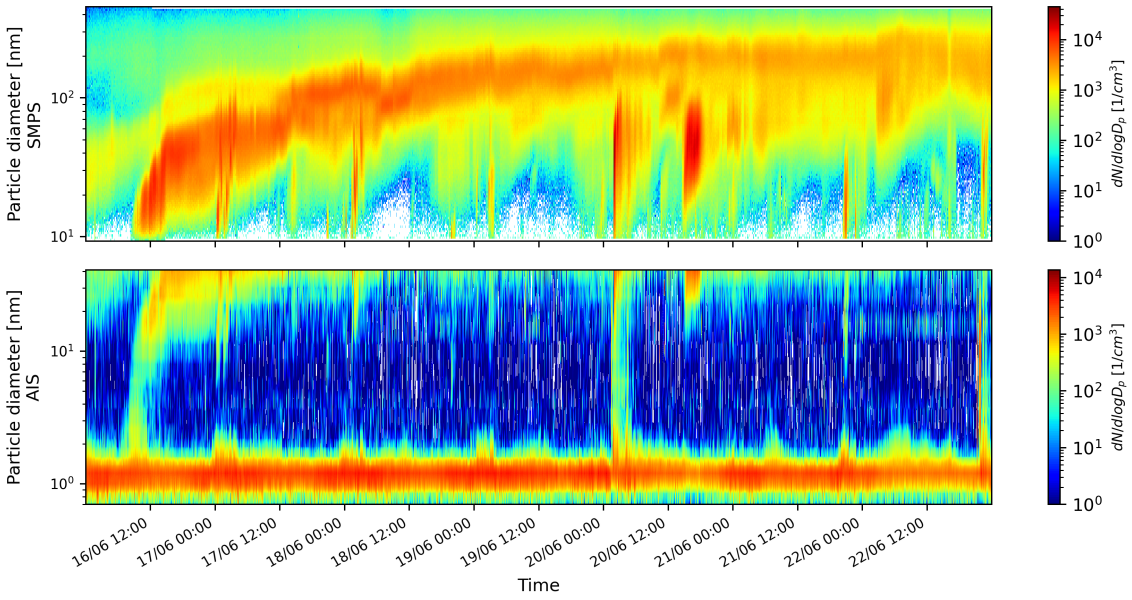

Fig. 29 Particle size distribution illustrating bananaplot for SMPS (top) and AIS (bottom) during new particle formation event 2022 June 16-22 in Abisko measurement station

3.3.2 New particle formation events

During the 61 days with data it was found in total 17 NPF events, 16 undefined and 28 non-events. Their frequency for the different months are presented in Fig. 30, with event frequency peak in July. In August, the frequency was very low which can partly be explained by 14 overall days with data and only half of the month presented. Table 6 shows the numbers of the different categories as well as the median lengths. This study found NPF during 22% of days during June,

37% during July and 21% during August. Compared to Svenningsson et al. [72], where equivalent measurements were performed at the same site in 2005 and 2006, the 2023 NPF event frequency was significantly lower. Svenningsson et al. [72] report event frequency of 50% or above for the summer months while this study found around 30% occurrence overall. In this case by considering both event and undefined days as NPF event days, results would be similar to 2005 and 2006 data, meaning recalculated NPF during June - 52 %, July - 70 %, August - 29 %.

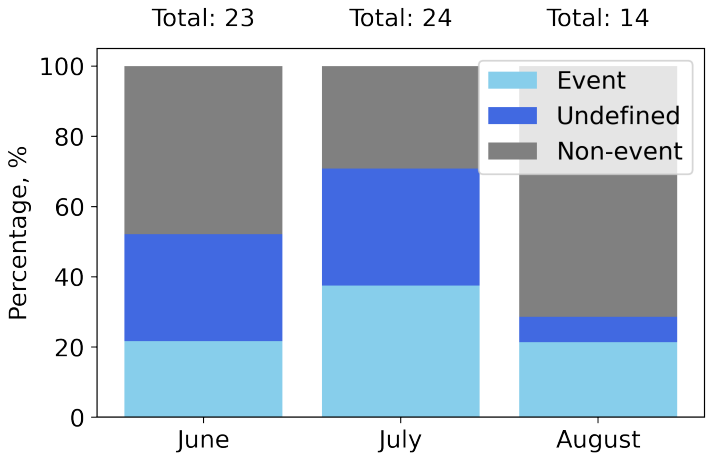

Fig. 30 Frequency of new particle formation event occurrence and the total of measurement days (top) during summer of 2023 (Abisko, Sweden)

Table 6 Number of NPF events, undefined and non-events, total days during summer of 2023 (June, July, August and overall) as well as event and undefined median lengths in hours (Abisko, Sweden).

Month	Event	Undefined	Non-event	Total	Event length median [h]	Undefined length median [h]
June	5	7	11	23	10	12
July	9	8	7	24	20	2
August	3	1	10	14	24	20
All months	17	16	28	61	20	12

New particle formation events were most often observed during daytime (around 90%), as it is presented in Fig. 31, where the growth rate for the 17 events is plotted as a function of onset time and split into wind direction from the east and west. The overall growth rates consistently remained below 10 nm/h, although there were occasional outliers during daytime. This is concurrent with the theory some common biogenic volatile organic compounds (BVOCs) being emitted from the trees as they are exposed to sunlight, which are then oxidized into low volatile compounds that can condense into new or grow on small particles [75]. Secondly, it was obeserved that events occurring during nighttime are likely to have higher growth rate, two NPF events occurred at 2 a.m. and 4 a.m. with growth rates of 13.9 nm/h and 11.6 nm/h, accordingly. Similar results was reported by Svenningsson et al. [72], supporting the conclusion that night time NPF event indeed have higher

growth rate (over 10 nm/h). Finally, during daytime the growth rate was higher for easterly flow (GR 7.7 nm/h) compared to westerly flow growth rate (GR 4.0 nm/h).

Within the daytime events, the overall growth rate ranges were fairly similar compared to [72], staying below 10 nm/h with some outliers. However, Svenningsson et al. [72] found several events with growth rate ranging from 10 up to 50 nm/h (especially during nighttime), while this project found a maximum growth rate of approximately 13.9 nm/h. A major reason could be the subjective method by which we calculated the growth rates in this study. In Svenningsson et al. [72] each distribution was fitted with several log normal distributions from which the growth of the nucleation mode can be determined. Another possible reason for the differences is that nighttime events with short bursts of growth, were not classified as events in this study but rather fall into the undefined category. These types of events, exemplified by Fig. 29, would add more events with higher growth rates similar to the finding of Svenningsson et al. [72].

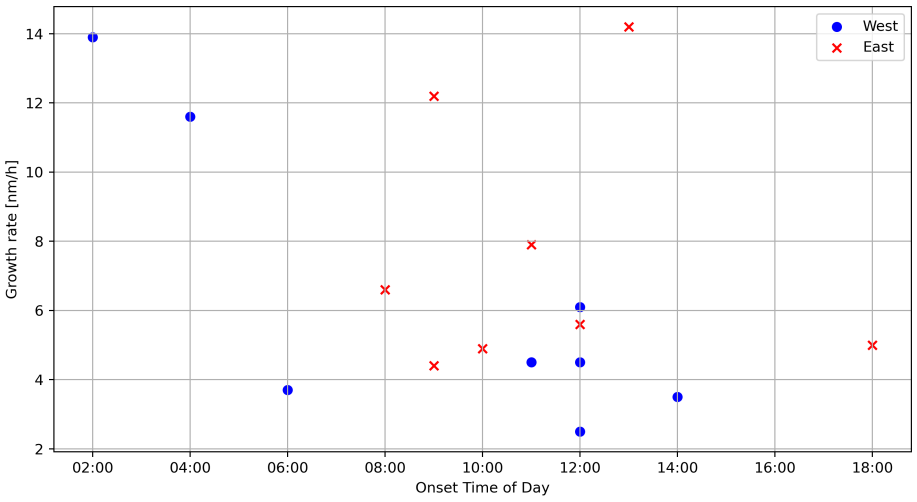

Fig. 31 Growth rate for the events as a function of onset time, measured with SMPS (Abisko, Sweden). The different colors and shapes indicate the dominant wind direction.

In this study, a peak NPF event frequency was found in July. This is confirmed by Svenningsson et al. [72], who also found a summer peak in NPF event frequencies at the same site, with 70% days of July classified as NPF events. This implied that the site experiences a shorter summer season, as well as a shorter growing season for tree leaves, with the season starting at the end of June and ending in the beginning of August, since the NPF frequency during autumn and spring was reported less than 30%. Seco at al. [76] showed that BVOCs fluxes from the fen surrounding the measurement site are almost nonexisting outside the growing season, while comprising a majority of the total volatile organic compound fluxes during July. This suggests that the increased NPF event frequency during summer indeed is due to BVOC emissions.

As seen in Table 6, the events were overall longer in time than undefined events. This reflected the the definitions of NPF events, which is partly based on a duration criteria. This is exemplified by Fig. 29, were the main events started at slightly before noon and grew clearly into the accumulation mode. The growth continued several days. However, during NPF events it was noticed several smaller bursts of particles in the nucleation mode moving into the Aitken mode in the span of one

or two hours, that most often occurred at night. Under definition of NPF event, it fall under the undefined category. In addition, Seco et al. [76] showed that the fluxes of some BVOCs peak at around noon, with zero fluxes at night. This lines up with the findings of both this project and [72], were a majority of events occur around noon.

Fig. 32 presents four meteorological variables from a weather station near the measuring site for the events onset time of day. As expected, it was found approximately two wind directions: 300 degrees and 130 degrees, indicating wind blowing along the Torneträsk valley from the Atlantic Ocean in the west or from the east. NPF dependence on temperature and net radiation showed a typical pattern, with peak NPF in the middle of the day (12h). Higher net radiation (more light) and temperature could lead to an increased emissions of BVOC [77] and a greater indication of NPF, as well as a higher growth rate [78]. Relative humidity also exhibited a typical pattern, with higher levels (90-100 %) at night and lower levels (50-90 %) in the middle of the day [79]. Fig. 33 presents the same but for growth rate. Here, it was noticed a weak correlation of higher growth rate with higher temperature and relative humidity. Also slightly higher rate for easterly flow as noted previously.

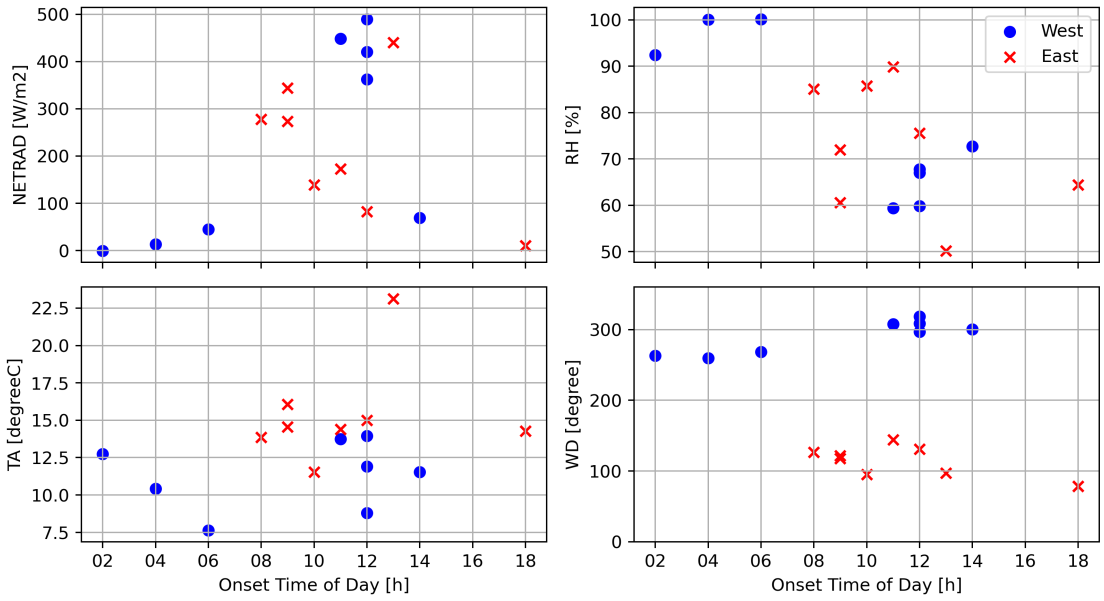

Fig. 32 The onset time of day for the NPF events plotted against four different meteorological variables, net radiation (top left), relative humidity (top right), air temperature (bottom left) and wind direction (bottom right) for summer, 2023 (Abisko, Sweden).

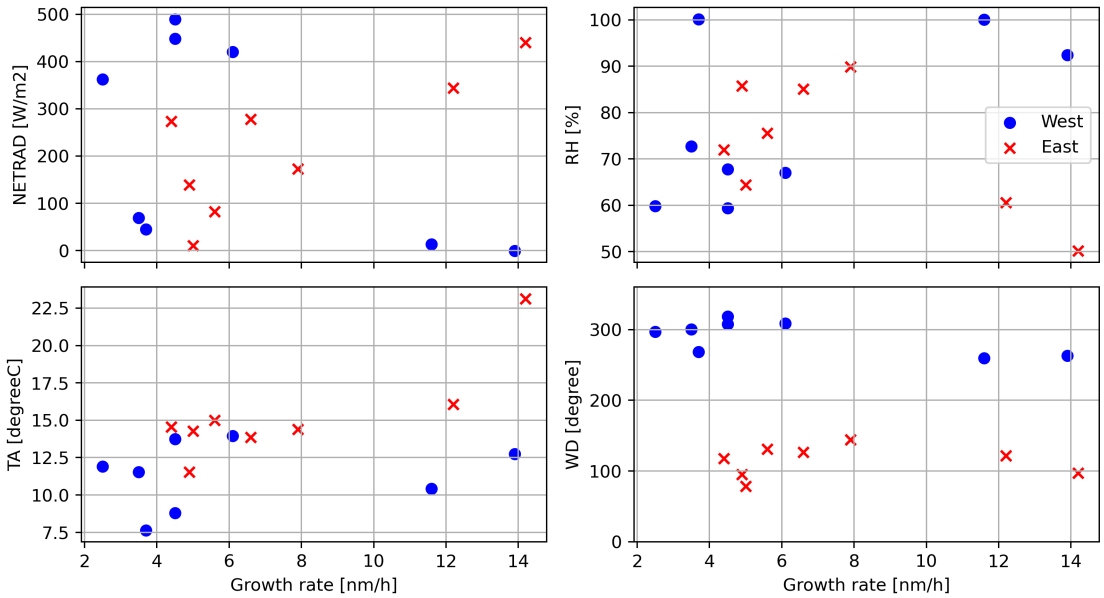

Fig. 33 The growth rate plotted against four different meteorological variables, net radiation (top left), relative humidity (top right), air temperature (bottom left) and wind direction (bottom right) for summer, 2023 (Abisko, Sweden).

3.4 Comparison of different datasets

Examining data from different locations allows for the identification of patterns or discrepancies, ultimately enhancing our understanding of the spatial variability of atmospheric processes. Statistical information provided in Figures 1, 24, and 30 revealed a consistent tendency due to seasonality. In Hyltemossa, around 60% or more of the days from March to October were classified as event days, while during colder periods (November to February), less than 40% of the days showed NPF events. Similarly, in the Abisko measurement station, during July and June, the warmest months of the year, more than 50% of the days were identified as event days (including undefiend days). In Vilnius, NPF occured 40-60 % from March to August and 10 - 30 % November - December. Thus, new particles are more likely to form during warmer seasons, as it stated in other studies as well [40, 50, 51]. In Vilnius urban background station NPF frequency was lower compared to rural and remote sites in Sweden - this tendency was observed in the literature as well [80, 81]. When comparing downtown Toronto (Ontario, Canada) with a rural station near Egbert (Ontario), it was found that nucleation events occurred more frequently in the rural site and hypothesized that this difference could be attributed to anthropogenic pollution, which may suppress nucleation events in urban areas [81]. Also similar NPF peaks was found, with around 60 % in rural environment and around 40 % in urban environment during May-June [81]. In urban environments, nucleation events tend to occur less frequently due to the higher concentrations of atmospheric pollutants (sulfur dioxide, nitrogen oxides, organic carbon), which have a negative impact on NPF [79]. However, when NPF do occur, it can be more intense, suggesting higher growth rates, meaning particles are capable of escaping coagulation scavenge and grow more rapidly in polluted air than in cleaner surroundings [80].

In Vilnius, calculated growth rate showed higher values, with median value 5.8 nm/h. In Hyl-

temossa the median growth rate was 3.9 nm/h and Abisko - 5.3 nm/h. In urban environments, it is expected to have higher growth rates [80]. By comparing urban and rural sites, it is reported that in urban sites, the growth rate is higher by a factor of 1.6 [80,82], which closely aligns with the comparison of growth rates between Vilnius and Hyltemossa (by a factor 1.5). For instance, in the Budapest urban measurement station, the mean growth rate was 7.7 nm/h, while in the K-puszta rural background station, the growth rate was 4.8 nm/h (in Hungary) [80]. It is explained that precursors for NPF are more abundant in urban sites compared to rural sites [82]. In the Abisko measurement station, the growth rate was calculated by the factor of 1.35 higher compared with Hyltemossa and 1.1 times lower than that of Vilnius. However, the growth rate in the Abisko measurement station was calculated using available data representing the summer of 2023, while data representing the entire year was available for Vilnius and Hyltemossa. This could influence that in the Abisko the growth rate parameter is less representative due to availability of the data. Also, in other studies [72] growth rates are determined using the log-normal distribution fitting method, which may represent a more advanced approach and yield more accurate calculations.

Seasonal number concentration variability between Sweden and Lithuania showed observable similarities. The highest number concentration is observed during spring with highest contribution from nucleation mode particles, meaning highest contribution came from new particle formation. Average annual aerosol particle number concentration value differed between sites, in Vilnius - 4560 cm^{-3}, in Hyltemossa - 2278 cm^{-3}. This showed clear difference between urban and forest environments.

The meteorological factors found to influence NPF comparing event and non-event days as well as influence submicronic aerosol size distribution. The level of solar radiation reaching the Earth's surface is the primary factor influencing the occurrence of NPF [53, 73], with an average increase of around 80 % in incoming shortwave radiation observed in Hyltemossa during NPF event days. Solar radiation enhances photochemical reactions, leading to the generation of aerosol precursors like sulfuric acid and non-volatile vapors, which can coagulate to form clusters and initiate new particle formation [79, 83, 84]. Another meteorological factor that influence NPF is relative humidity, which plays a negative role in promoting the formation of low-volatility organic compounds [53, 79]. This work shows that there was a negative correlation between nucleation mode concentration and relative humidity during event days (Spearman correlation coefficient - 0.54). Comparing event and non-event days provided a clear tendency for relative humidity to be lower during event days (average 80% during non-event and 70% during event days) in Vilnius site, very similar tendency was shown in Sweden Hyltemossa site (average 90% during non-event and 81% during event days). In Abisko project there was also identification that NPF followed relative humidity typical pattern, with RH higher levels at night and lower levels in the middle of the day. While water in the atmosphere is crucial for the formation of initial clusters in both binary and ternary nucleation theories [22], it can also reduce new particle formation by increasing aerosol surface area under certain atmospheric conditions [85]. While meteorological parameter are not independent, RH tends to decrease with increasing solar radiation and temperature [79]. A higher relative humidity (for example, during nighttime) has been shown to increase particle

growth rates across all sites (see Fig. 5, 27, 33). However, there is no clear tendency between relative humidity and growth rates, as also observed in other studies [79]. In this article [79], it is noted that meteorological parameters' relationships with growth rate vary significantly, with no clear tendency observed. Nevertheless, a positive relationship between growth rate and particulate organic carbon, volatile organic compounds, and particulate-phase sulfate was observed, although not studied in this thesis.

Another factors that can influence new particle formation was considered with using wind direction and temperature. Wind direction can have an impact by influencing the concentration of precursor gases and aerosols. This influence may be attributed to the fact that incoming air masses are influenced by various biogenic emissions and anthropogenic pollutants, as well as exposed to diverse meteorological conditions before reaching the measurement site [53]. In Vilnius site, there is indication that there is higher frequency of NPF when the wind prevails from the western direction, indicating that air masses originating from the Baltic Sea tend to be cleaner and cleaner air masses is a favorable condition for starting NPF as well as sunny conditions with low RH [86] (Fig. 4). Not only that but conditional probability analysis in Hyltemossa site (Fig. 23) shows indication of increased particle number concentration together with increased wind speed and wind direction from Baltic sea (western side). South-west direction dominates comparing event and non-event days in Hyltemossa as well, all together showing that marine air masses have influence on increased occurrence of NPF both in Vilnius and Hyltemossa sites. Another meteorological factor to consider is ambient temperature, which also exhibits a tendency in relation to NPF. Analysis across all sites revealed that on event days, temperatures tend to be higher compared to non-event days, and NPF occurrences tend to be more frequent during daytime, coinciding with increased temperatures. Overall, new particle formation exhibits a seasonal trend, typically increasing during warmer periods and decreasing in autumn and winter months. In other studies, the relationship between temperature and NPF is not consistently positive or negative, likely due to the influence of various temperature-dependent mechanisms, such as the formation of molecular clusters from various precursor vapors, the growth of newly formed particles, or particle evaporation [53, 79]. Despite decades of intensive studies, the processes behind the occurrence and evolution of new particle formation events remain mostly unclear and shows the need for further research.

4 Main Results and Conclusions

1. The study of data from the ACTRIS station in Hyltemossa, Sweden, provides insights into aerosol measurement reliability. Addressing discrepancies with closure studies revealed reasonable agreement for used instruments' datasets and significantly enhanced ACTRIS data quality. The study shows that it is non-trivial to measure ambient air concentration with a single instrument, emphasizing the need for multiple instruments, regular calibration, and intercomparison to ensure accuracy and station reliability.

2. In Vilnius, Hyltemossa, and Abisko measurement stations, new particle formation occurred 40-60% of the time during the warmest seasons. This period spanned March to October in Vilnius and Hyltemossa, and June to July in Abisko due to different climate factors. NPF was more prevalent during warmer seasons and revealed a consistent trend with seasonality. NPF was less frequent in Vilnius compared to rural and remote Swedish sites, likely due to urban pollution. However, NPF events were more intense in Vilnius, with median growth rates 1.5 times higher than in Hyltemossa, consistent with literature comparisons [80, 82].

3. Meteorological factors significantly influence new particle formation. At the Hyltemossa site, solar radiation was higher by 80% on NPF event days, while relative humidity was lower compared with non-event days at all sites. Wind direction and air mass origin exhibit significant correlations with NPF frequency; it decreases with continental air masses and increases with marine air masses in Vilnius and Hyltemossa. Further studies are needed to investigate these influencing factors.

4. The analysis of seasonal behavior demonstrated winter lows and spring peaks in aerosol number concentrations. From March 2022 to February 2023, the average submicron aerosol particle number concentration in Vilnius's urban background was 4560 cm^{-3}, which is lower than in many other European cities. In contrast, measurements from Hyltemossa and Abisko showed lower average concentrations, indicating cleaner environments in these Swedish forest and rural locations compared to the urban background in Vilnius.

This study reveals the factors influencing submicrometer aerosol dynamics in urban, remote and sub-arctic forest environments, emphasizing the complexity and importance of aerosol particle formation.

5 List of publications and conferences

Publications:

1. L. Davulienė, L. Janicka, A. Minderytė, A. Kalinauskaitė, P. Poczta, M. Karasewicz, A. Hafiz, D. Pashneva, V. Dudoitis, **K. Kandrotaitė**, ... S. Byčenkienė. Synergic use of in-situ and remote sensing techniques for comprehensive characterization of aerosol optical and microphysical properties. Science of the Total Environment (2024) 906, 167585. DOI: https://doi.org/10.1016/j.scitotenv.2023.167585

2. L. Davulienė, A. Khan, S. Šemčuk, A. Minderytė, M. Davtalab, **K. Kandrotaitė**, V. Dudoitis, I. Uogintė, M. Skapas, S. Byčenkienė, Evaluation of work-related personal exposure to aerosols particles, Toxics (2022). DOI: https://doi.org/10.3390/toxics10070405.

3. **K. Kandrotaitė**, V. Dudoitis, I. Uogintė, P. Strizak, F. Pope, K. Plauškaitė, S. Byčenkienė, Aerosol filtration efficiency of common fabrics used in cloth masks in Lithuania, Lithuanian Journal of Physics (2022). DOI: https://doi.org/10.3952/physics.v62i2.4743

4. A. Khan, L. Davulienė, S. Šemčuk, **K. Kandrotaitė**, A. Minderytė, M. Davtalab, ... S. Byčenkienė. Integrated personal exposure and deposition of black carbon on human lungs. Air Quality, Atmosphere Health (2023), 17(1), 35-50. DOI: https://doi.org/10.1007/s11869-023-01428-8

5. T. Gill, S. Kecorius, **K. Kandrotaitė**, V. Dudoitis, L. Madueño, A. Wiedensohler, L. Poulain, E. Vallar, M. Galvez, S. Byčenkienė, K. Plauškaitė. Carbonaceous aerosol particle sources in Manila North Port and urban environment. Atmospheric Pollution Research. (Manuscript unpublished, submitted to the editors).

Conference Presentations:

1. K. Kandrotaitė, V. Dudoitis, S. Byčenkienė, New particle formation events in urban background environment in Vilnius, Lithuania, European Aerosol Conference, September 3-8, 2023 Malaga, Spain (poster presentation).

2. K. Kandrotaitė, A. Minderytė, J. Pauraitė, L. Davulienė, D. Valiulis, F. Mirza-Montoro, P. Poczta, R. Fortuna, E. Ugboma, L. Janicka, D. Szczepanik, I. S. Stachlewska, S. Byčenkienė, BIOSURE - Importance of long-range transport of BIOmass burning emissions to local Smog events in Urban Environments, International Aerosol Conference, September 4-9, 2022, Athens, Greece (poster presentation).

3. K. Kandrotaitė, L. Davulienė, Itin smulkių aerozolio dalelių dinamikos ypatumus lemiančių veiksnių tyrimai, Studentų mokslinė konferencija 2024: Studentų tyrimų semestrų metu 23/24 m.“, May 16-17, 2024 (oral presantation).

4. K. Kandrotaitė, S. Byčenkienė, Submikroninių aerozolio dalelių dinaminių vyksmų tyrimai miesto aplinkoje, Studentų mokslinė konferencija 2023: Naujoji mokslininkų karta", April 18d, 2023 (oral presantation).

5. K. Kandrotaitė, A. Minderytė, A. Kalinauskaitė, L. Davulienė, L. Janicka, V. Dudoitis, I. S. Stachlewska, S. Byčenkienė, Aerosol particle number concentration and size distribution during Midsummer event, Open Readings 2023, April 18–21, 2023, Vilnius (poster presentation).

6. K. Kandrotaitė, L. Davulienė, A. Khan, S. Šemčiuk, A. Minderytė, M. Davtalab, V. Dudoitis, I. Uogintė, M. Skapas and S. Byčenkienė, Evaluation of work-related personal exposure to aerosol particles, 12-ji Fizinių ir technologijos mokslų centro doktorantų ir jaunųjų mokslininkų konferencija FizTech, October 19-20, 2022, Vilnius (poster presentation).

7. A. Minderytė, K. Kandrotaitė, A. Kalinauskaitė, L. Davulienė, L. Janicka, V. Dudoitis, I. S. Stachlewska, S. Byčenkienė, A case study of extensive biomass burning related black carbon emissions during Midsummer Eve in Vilnius, Lithuania, Nordic Society for Aerosol Research: NOSA, March 13-15, 2023, Oslo, Norway (poster presentation).

8. K. Kandrotaitė, S. Byčenkienė, A. Kilikevičius, J. Matijošius, K. Plauškaitė, Akustinis ultrasmulkiųjų dalelių filtras dujų išmetimo sistemoms, 45-oji Lietuvos nacionalinė fizikos konferencija, October 25-27, 2023, Vilnius, (poster presentation).

Submikroninių aerozolio dalelių dinaminių vyksmų tyrimas

Kamilė Kandrotaitė

Santrauka

Oro tarša yra viena didžiausių sveikatos problemų sukėlėja pasaulyje, dėl kurios kasmet miršta apie 7 milijonai žmonių. Aerozolio dalelės, svarbi oro taršos sudedamoji dalis, yra tyrinėjamos dėl žalingo poveikio žmonių sveikatai, ypač dėl savybės giliai įsiskverbti į kvėpavimo takų sistemą. Didelę sveikatos riziką kelia mažesnės nei 1 um (submikroninio dydžio) dalelės, kurios turi didelę nusėdimo tikimybę bronchų srityje, alveolėse bei kraujotakoje. Be to, aerozolio dalelių sąveika su saulės spinduliuote daro įtaką Žemės klimatui ir atmosferai. Aerozolio dalelės, priklausomai nuo jų fizikinių ir cheminių savybių, gali išsklaidyti ar sugerti spinduliuotę, todėl tiesiogiai paveikia bendrą Žemės energijos balansą. Taip pat stebimas ir netiesioginis poveikis dėl aerozolio dalelių, pasireiškiantis per kintančias debesų savybes, prailginant debesų gyvavimo laiką ar modifikuojant albedo.

Tyrinėjant aerozolių vaidmenį žmonių sveikatos srityje, atmosferos procesuose ir klimato dinamikoje, svarbu suprasti kaip susidaro aerozolio dalelės. Naujų dalelių susidarymas yra savaimine vykstantis procesas atmosferoje, didinantis dalelių skaičiaus koncentraciją foninėje aplinkoje. Tiriant naujų dalelių susidarymą gaunama įžvalgų apie įvairius atmosferos procesus, įskaitant submikrometrinių dalelių susidarymą, jų augimą dėl kondensacinių ar koaguliacinių procesų. Šiame tyrime pagrindinis dėmesys skiriamas trijų skirtingų vietovių duomenų analizei: miesto Vilniuje (Lietuvoje) ir miško (atokiose) vietovėse Hyltemossa ir Abisko (Švedija). Lyginamoji šių duomenų analizė leidžia daryti išvadas apie erdvinį ir sezoninį aerozolių dinamikos kintamumą. Tyrimu siekiama palyginti submikrometrinių dalelių ir naujų dalelių susidaromo epizodų pasiskirstymą šiose vietose – tokio tipo palyginimas dar nebuvo atliktas Šiaurės Europos šalyse.

Šio darbo tikslas – išanalizuoti submikroninių aerozolio dalelių dydžio pasiskirstymo duomenis ir jų dinamiką Vilniaus miesto foninio lygio matavimo stotyje ir palyginti juos su Šiaurinės Europos matavimo stočių, Hyltemossa jūrinio klimato matavimo stoties ir subarktinio žemyninio klimato Abisko stoties duomenimis. Tikslui pasiekti suformuluoti šie uždaviniai: (1) Atlikti Hyltemossa matavimo stoties prietaisų veikimo ir registruojamų duomenų nuoseklumo palyginamąją analizę, vertinant skirtingus aerozolių matavimo prietaisus dėl kritinių aerozolių savybių; (2) nustatyti naujų dalelių susidarymą bei kiekybiškai įvertinti susidarymo epizodų dažnumą bei dalelių augimo greičius; (3) analizuoti ir nustatyti naujų aerozolių dalelių susidarymą lemiančius veiksnius; (4) palyginti submikrometrinių aerozolio dalelių koncentracijos dinamiką tarp stebėjimo stočių atitinkančių skirtingą foninį lygį (miesto, kaimo, atoki vietovė).

Hyltemossa matavimų stoties duomenų tyrimas suteikia įžvalgų apie aerozolio dalelių matavimo duomenų patikimumą. Tyrimas parodo, kad aplinkos aerozolio dalelių koncentracijos matavimai vienu prietaisu negali būti pilnai patikimi. Kelių prietaisų naudojimas, kalibravimas ir matavimo duomenų tarpusavio palyginimas, užtikrina matavimo duomenų patikimumą.

Vilniaus, Hyltemossa ir Abisko matavimo stotyse šilčiausiais metų laikais naujų dalelių susidarymo epizodai nustatyti 40-60% matuotų parų. Naujų dalelių susidarymo epizodai buvo dažnesni šiltesni-

ais sezonais ir atskleidė sezoniškumo tendencijas. Vilniuje nustatyta mažiau naujų dalelių formavimosi epizodų, tačiau čia naujų dalelių susidarymo epizodai nustatyti intensyvesni, augimo greičių mediana buvo 1,5 karto didesnė nei Hyltemossa matavimų stotyje, panašūs rezultatai pateikiami ir literatūroje.

Pagrindinis meteorologinis veiksnys, saulės spinduliuotės intensyvumas naujų dalelių susidarymo dienomis yra didesnis iki 80% lyginant su kitomis dienomis. Santykinė oro drėgmė nustatyta žemesnė naujų dalelių susidarymo dienomis. Vėjo kryptis ir oro masių pernaša iš jūrinės pusės padidina nukleacijos tikimybę.

Vidutinė metinė submikroninių aerozolių dalelių skaičiaus koncentracija Vilniaus miesto foninėje aplinkoje nustatyta 4560 cm^{-3}, tai yra mažesnė nei daugelyje kitų Europos miestų. Kita vertus, Hyltemossa ir Abisko matavimai pasižymėjo mažesnėmis vidutinėmis koncentracijomis.

Šis tyrimas atskleidžia veiksnius, turinčius įtakos submikrometro aerozolių dinamikai miesto, miško ir atokioje subarktinėje aplinkoje, pabrėžiant aerozolio dalelių susidarymo sudėtingumą ir svarbą.

References

[1] H. Ritchie and M. Roser, Air pollution, *Our World in Data*, 2024.

[2] W. H. Organization, *Burden of disease from the joint effects of household and ambient air pollution for 2016, Social and Environmental Determinants of Health Department, Geneva*. 2016.

[3] M. Park, H. S. Joo, K. Lee, *et al.*, Differential toxicities of fine particulate matters from various sources, *Scientific reports*, 2018, **8**, 17007.

[4] S. Ohlwein, R. Kappeler, M. Kutlar Joss, N. Künzli, and B. Hoffmann, Health effects of ultrafine particles: a systematic literature review update of epidemiological evidence, *International journal of public health*, 2019, **64**, 547–559.

[5] A. E. Haddrell, D. Lewis, T. Church, R. Vehring, D. Murnane, and J. P. Reid, Pulmonary aerosol delivery and the importance of growth dynamics, *Therapeutic delivery*, 2017, **8**, 1051–1061.

[6] H.-S. Kwon, M. H. Ryu, and C. Carlsten, Ultrafine particles: unique physicochemical properties relevant to health and disease, *Experimental & molecular medicine*, 2020, **52**, 318–328.

[7] R. A. Kahn, E. Andrews, C. A. Brock, *et al.*, Reducing aerosol forcing uncertainty by combining models with satellite and within-the-atmosphere observations: A three-way street, *Reviews of Geophysics*, 2023, **61**, e2022RG000796.

[8] G. Myhre, C. Myhre, B. Samset, and T. Storelvmo, Aerosols and their relation to global climate and climate sensitivity, *Nature Education Knowledge*, 2013, **4**, 7.

[9] V. Groma, B. Alföldy, E. Börcsök, *et al.*, Sources and health effects of fine and ultrafine aerosol particles in an urban environment, *Atmospheric Pollution Research*, 2022, **13**, 101302.

[10] T. Arfin, A. M. Pillai, N. Mathew, A. Tirpude, R. Bang, and P. Mondal, An overview of atmospheric aerosol and their effects on human health, *Environmental Science and Pollution Research*, 2023, **30**, 125347–125369.

[11] D. E. Schraufnagel, The health effects of ultrafine particles, *Experimental & molecular medicine*, 2020, **52**, 311–317.

[12] J. Li, B. E. Carlson, Y. L. Yung, *et al.*, Scattering and absorbing aerosols in the climate system, *Nature Reviews Earth & Environment*, 2022, **3**, 363–379.

[13] W. C. Hinds, *Aerosol technology*. John Wiley Sons, 1999.

[14] S. Twomey, The influence of pollution on the shortwave albedo of clouds, *Journal of the atmospheric sciences*, 1977, **34**, 1149–1152.

[15] D. Liu, C. He, J. P. Schwarz, and X. Wang, Lifecycle of light-absorbing carbonaceous aerosols in the atmosphere, *NPJ Climate and Atmospheric Science*, 2020, **3**, 40.

[16] W. H. Organization *et al.*, *WHO global air quality guidelines: particulate matter (PM2. 5 and PM10), ozone, nitrogen dioxide, sulfur dioxide and carbon monoxide*. World Health Organization, 2021.

[17] S. Ohlwein, R. Kappeler, M. Kutlar Joss, N. Künzli, and B. Hoffmann, Health effects of ultrafine particles: a systematic literature review update of epidemiological evidence, *International journal of public health*, 2019, **64**, 547–559.

[18] S. Kecorius, L. Madueño, J. Löndahl, *et al.*, Respiratory tract deposition of inhaled roadside ultrafine refractory particles in a polluted megacity of south-east asia, *Science of the Total Environment*, 2019, **663**, 265–274.

[19] S. Armalis, *Atmosferos chemija*. Vilniaus universiteto ledykla, 2009.

[20] M. U. Ali, S. Lin, B. Yousaf, *et al.*, Pollution characteristics, mechanism of toxicity and health effects of the ultrafine particles in the indoor environment: Current status and future perspectives, *Critical Reviews in Environmental Science and Technology*, 2022, **52**, 436–473.

[21] M. Kulmala, J. Kontkanen, H. Junninen, *et al.*, Direct observations of atmospheric aerosol nucleation, *Science*, 2013, **339**, 943–946.

[22] M. Kulmala, How particles nucleate and grow, *Science*, 2003, **302**, 1000–1001.

[23] A. Wiedensohler, W. Birmili, A. Nowak, *et al.*, Mobility particle size spectrometers: harmonization of technical standards and data structure to facilitate high quality long-term observations of atmospheric particle number size distributions, *Atmospheric Measurement Techniques*, 2012, **5**, 657–685.

[24] E. Knutson and K. Whitby, Aerosol classification by electric mobility: apparatus, theory, and applications, *Journal of Aerosol Science*, 1975, **6**, 443–451.

[25] G. Roberts and A. Nenes, A continuous-flow streamwise thermal-gradient ccn chamber for atmospheric measurements, *Aerosol Science and Technology*, 2005, **39**, 206–221.

[26] D. Rose, S. Gunthe, E. Mikhailov, G. Frank, U. Dusek, M. O. Andreae, and U. Pöschl, Calibration and measurement uncertainties of a continuous-flow cloud condensation nuclei counter (dmt-ccnc): Ccn activation of ammonium sulfate and sodium chloride aerosol particles in theory and experiment, *Atmospheric Chemistry and Physics*, 2008, **8**, 1153–1179.

[27] CCNC manual, *Cloud Condensation Nuclei (CCN) Counter - Manual for Single-Column CCNs DOC0086 Revision 1-2*. Droplet Measurement Technologies LLC.

[28] FIDAS manual, *Operating Manual Fine Dust Monitor System*. PALAS GmbH, 2021.

[29] W. P. Arnott, K. Hamasha, H. Moosmüller, P. J. Sheridan, and J. A. Ogren, Towards aerosol light-absorption measurements with a 7-wavelength aethalometer: Evaluation with a photoacoustic instrument and 3-wavelength nephelometer, *Aerosol Science and Technology*, 2005, **39**, 17–29.

[30] Aethalometer manual, *Aethalometer® Model AE33 User Manual*. Magee Scientific , 2021.

[31] T. B. Watson, Aerosol chemical speciation monitor (acsm) instrument handbook, tech. rep., DOE Office of Science Atmospheric Radiation Measurement (ARM) Program, 2017.

[32] N. L. Ng, S. C. Herndon, A. Trimborn, *et al.*, An aerosol chemical speciation monitor (acsm) for routine monitoring of the composition and mass concentrations of ambient aerosol, *Aerosol Science and Technology*, 2011, **45**, 780–794.

[33] M. Canagaratna, J. Jayne, J. Jimenez, *et al.*, Chemical and microphysical characterization of ambient aerosols with the aerodyne aerosol mass spectrometer, *Mass Spectrometry Reviews*, 2007, **26**, 185–222.

[34] A. Mirme, E. Tamm, G. Mordas, *et al.*, A wide-range multi-channel air ion spectrometer, 2007.

[35] X. Chen, A. Virkkula, V.-M. Kerminen, *et al.*, Features in air ions measured by an air ion spectrometer (ais) at dome c, *Atmospheric Chemistry and Physics*, 2017, **17**, 13783–13800.

[36] E. Asmi, M. Sipilä, H. Manninen, *et al.*, Results of the first air ion spectrometer calibration and intercomparison workshop, *Atmospheric Chemistry and Physics*, 2009, **9**, 141–154.

[37] AIREL Ltd., *Air Ion spectrometer AIS. Serial no. 3. Operation Manual*. Institute of Environmental Physics, University of Tartu.

[38] M. Canagaratna, J. Jayne, J. Jimenez, *et al.*, Chemical and microphysical characterization of ambient aerosols with the aerodyne aerosol mass spectrometer, *Mass spectrometry reviews*, 2007, **26**, 185–222.

[39] M. Dal Maso, M. Kulmala, I. Riipinen, R. Wagner, T. Hussein, P. P. Aalto, and K. E. Lehtinen, Formation and growth of fresh atmospheric aerosols: eight years of aerosol size distribution data from smear ii, hyytiälä, finland, *Boreal environment research*, 2005, **10**, 323.

[40] Z. Németh, B. Rosati, N. Zíková, *et al.*, Comparison of atmospheric new particle formation events in three central european cities, *Atmospheric Environment*, 2018, **178**, 191–197.

[41] R. Weber, P. McMurry, F. Eisele, and D. Tanner, Measurement of expected nucleation precursor species and 3–500-nm diameter particles at mauna loa observatory, hawaii, *Journal of Atmospheric Sciences*, 1995, **52**, 2242–2257.

[42] G. Mordas, K. Plauškaitė, N. Prokopčiuk, V. Dudoitis, C. Bozzetti, and V. Ulevicius, Observation of new particle formation on curonian spit located between continental europe and scandinavia, *Journal of Aerosol Science*, 2016, **97**, 38–55.

[43] V. Čekanavičius and G. Murauskas, Statistika ir jos taikymai: vadovėlis aukštųjų mokyklų studentams, *TEV, Vilnius*, 2006.

[44] P. Schober, C. Boer, and L. A. Schwarte, Correlation coefficients: appropriate use and interpretation, *Anesthesia & analgesia*, 2018, **126**, 1763–1768.

[45] I. S. Dar and S. Chand, Bootstrap-quantile ridge estimator for linear regression with applications, *Plos one*, 2024, **19**, e0302221.

[46] M. R. Chernick and R. A. LaBudde, *An introduction to bootstrap methods with applications to R*. John Wiley & Sons, 2014.

[47] R. R. Draxler and G. Hess, An overview of the hysplit_4 modelling system for trajectories, *Australian meteorological magazine*, 1998, **47**, 295–308.

[48] I. Šauliene and L. Veriankaite, Application of backward air mass trajectory analysis in evaluating airborne pollen dispersion, *Journal of Environmental engineering and landscape management*, 2006, **14**, 113–120.

[49] E. Alonso-Blanco, F. J. Gómez-Moreno, B. Artíñano, *et al.*, Temporal and spatial variability of atmospheric particle number size distributions across spain, *Atmospheric environment*, 2018, **190**, 146–160.

[50] T. Borsós, D. Řimnáčová, V. Ždímal, *et al.*, Comparison of particulate number concentrations in three central european capital cities, *Science of the total environment*, 2012, **433**, 418–426.

[51] H. Manninen, T. Nieminen, E. Asmi, *et al.*, Eucaari ion spectrometer measurements at 12 european sites–analysis of new particle formation events, *Atmospheric Chemistry and Physics*, 2010, **10**, 7907–7927.

[52] A. Hamed, J. Joutsensaari, S. Mikkonen, *et al.*, Nucleation and growth of new particles in po valley, italy, *Atmospheric Chemistry and Physics*, 2007, **7**, 355–376.

[53] V.-M. Kerminen, X. Chen, V. Vakkari, T. Petäjä, M. Kulmala, and F. Bianchi, Atmospheric new particle formation and growth: review of field observations, *Environmental Research Letters*, 2018, **13**, 103003.

[54] V. Dudoitis, G. Mordas, S. Byčenkienė, *et al.*, Aerosol particle formation in the lithuanian hemi-boreal forest, *Lithuanian Journal of Physics*, 2018, **58**, 283–293.

[55] D. Bousiotis, F. D. Pope, D. Beddows, *et al.*, A phenomenology of new particle formation (npf) at 13 european sites, *Atmospheric Chemistry and Physics*, 2021, **21**, 11905–11925.

[56] M. Zandersen, K. Hyytiäinen, H. M. Meier, *et al.*, Shared socio-economic pathways extended for the baltic sea: exploring long-term environmental problems, *Regional Environmental Change*, 2019, **19**, 1073–1086.

[57] M. Nekoro, State of the baltic sea: Background paper, 2013.

[58] K. Dimitriou and P. Kassomenos, Background concentrations of benzene, potential long range transport influences and corresponding cancer risk in four cities of central europe, in relation to air mass origination, *Journal of environmental management*, 2020, **262**, 110374.

[59] T. Gill, J. Pauraitė, A. Kalinauskaitė, S. Byčenkienė, and K. Plauškaitė, Long-term study of chemical characteristics of aerosol compositions in the rural environment of rūgšteliškis (lithuania), *Atmospheric Pollution Research*, 2024, **15**, 102048.

[60] P. Tunved, E. Nilsson, H.-C. Hansson, J. Ström, M. Kulmala, P. Aalto, and Y. Viisanen, Aerosol characteristics of air masses in northern europe: Influences of location, transport, sinks, and sources, *Journal of Geophysical Research: Atmospheres*, 2005, **110**.

[61] I. Rivas, D. C. Beddows, F. Amato, *et al.*, Source apportionment of particle number size distribution in urban background and traffic stations in four european cities, *Environment international*, 2020, **135**, 105345.

[62] S. D. Harni, S. Saarikoski, J. Kuula, *et al.*, Effects of emission sources on the particle number size distribution of ambient air in the residential area, *Atmospheric Environment*, 2023, **293**, 119419.

[63] S. J. Harris and M. M. Maricq, Signature size distributions for diesel and gasoline engine exhaust particulate matter, *Journal of Aerosol Science*, 2001, **32**, 749–764.

[64] M. Hu, J. Peng, K. Sun, D. Yue, S. Guo, A. Wiedensohler, and Z. Wu, Estimation of size-resolved ambient particle density based on the measurement of aerosol number, mass, and chemical size distributions in the winter in beijing, *Environmental science & technology*, 2012, **46**, 9941–9947.

[65] B. J. Turpin and H.-J. Lim, Species contributions to pm2. 5 mass concentrations: Revisiting common assumptions for estimating organic mass, *Aerosol Science & Technology*, 2001, **35**, 602–610.

[66] P. Tunved, H.-C. Hansson, M. Kulmala, *et al.*, One year boundary layer aerosol size distribution data from five nordic background stations, *Atmospheric Chemistry and Physics*, 2003, **3**, 2183–2205.

[67] M. D. Maso, A. Hyvärinen, M. Komppula, *et al.*, Annual and interannual variation in boreal forest aerosol particle number and volume concentration and their connection to particle formation, *Tellus B: Chemical and Physical Meteorology*, 2008, **60**, 495–508.

[68] S. Saarikoski, J. V. Niemi, M. Aurela, L. Pirjola, A. Kousa, T. Rönkkö, and H. Timonen, Sources of black carbon at residential and traffic environments obtained by two source apportionment methods, *Atmospheric Chemistry and Physics*, 2021, **21**, 14851–14869.

[69] R. Cichowicz, G. Wielgosiński, and W. Fetter, Dispersion of atmospheric air pollution in summer and winter season, *Environmental monitoring and assessment*, 2017, **189**, 1–10.

[70] M. Ketzel, P. Wåhlin, A. Kristensson, E. Swietlicki, R. Berkowicz, O. Nielsen, and F. Palmgren, Particle size distribution and particle mass measurements at urban, near-city and rural level in the copenhagen area and southern sweden, *Atmospheric Chemistry and Physics*, 2004, **4**, 281–292.

[71] E. Ahlberg, S. Ausmeel, L. Nilsson, *et al.*, Measurement report: Black carbon properties and concentrations in southern sweden urban and rural air–the importance of long-range transport, *Atmospheric Chemistry and Physics*, 2023, **23**, 3051–3064.

[72] B. Svenningsson, A. Arneth, S. Hayward, *et al.*, Aerosol particle formation events and analysis of high growth rates observed above a subarctic wetland–forest mosaic, *Tellus B: Chemical and Physical Meteorology*, Jan 2008.

[73] M. Kulmala and V.-M. Kerminen, On the formation and growth of atmospheric nanoparticles, *Atmospheric Research*, 2008, **90**, 132–150.

[74] M. Pikridas, J. Sciare, F. Freutel, *et al.*, In situ formation and spatial variability of particle number concentration in a european megacity, *Atmospheric Chemistry and Physics*, 2015, **15**, 10219–10237.

[75] M. Šimpraga, R. P. Ghimire, D. Van Der Straeten, *et al.*, Unravelling the functions of biogenic volatiles in boreal and temperate forest ecosystems, *European Journal of Forest Research*, 2019, **138**, 763–787.

[76] R. Seco, T. Holst, M. S. Matzen, *et al.*, Volatile organic compound fluxes in a subarctic peatland and lake, *Atmospheric Chemistry and Physics*, 2020, **20**, 13399–13416.

[77] R. Vella, A. Pozzer, M. Forrest, J. Lelieveld, T. Hickler, and H. Tost, Changes in biogenic volatile organic compound emissions in response to the el niño–southern oscillation, *Biogeosciences*, 2023, **20**, 4391–4412.

[78] A. Wonaschütz, A. Demattio, R. Wagner, *et al.*, Seasonality of new particle formation in vienna, austria–influence of air mass origin and aerosol chemical composition, *Atmospheric Environment*, 2015, **118**, 118–126.

[79] D. Bousiotis, J. Brean, F. D. Pope, *et al.*, The effect of meteorological conditions and atmospheric composition in the occurrence and development of new particle formation (npf) events in europe, *Atmospheric Chemistry and Physics*, 2021, **21**, 3345–3370.

[80] I. Salma, Z. Németh, V.-M. Kerminen, *et al.*, Regional effect on urban atmospheric nucleation, *Atmospheric Chemistry and Physics*, 2016, **16**, 8715–8728.

[81] Y.-S. Jun, C.-H. Jeong, K. Sabaliauskas, W. R. Leaitch, and G. J. Evans, A year-long comparison of particle formation events at paired urban and rural locations, *Atmospheric Pollution Research*, 2014, **5**, 447–454.

[82] Z. Wang, M. Hu, J. Sun, *et al.*, Characteristics of regional new particle formation in urban and regional background environments in the north china plain, *Atmospheric Chemistry and Physics*, 2013, **13**, 12495–12506.

[83] H. Wu, Z. Li, H. Li, *et al.*, The impact of the atmospheric turbulence-development tendency on new particle formation: a common finding on three continents, *National science review*, 2021, **8**, nwaa157.

[84] K. Wang, X. Ma, R. Tian, and F. Yu, Analysis of new particle nucleation events and comparisons to simulations of particle number concentrations based on geos-chem/apm in beijing, china, *Atmospheric Chemistry and Physics Discussions*, 2022, **2022**, 1–31.

[85] X. Li, S. Chee, J. Hao, J. P. Abbatt, J. Jiang, and J. N. Smith, Relative humidity effect on the formation of highly oxidized molecules and new particles during monoterpene oxidation, *Atmospheric Chemistry and Physics*, 2019, **19**, 1555–1570.

[86] M. Peltola, C. Rose, J. V. Trueblood, S. Gray, M. Harvey, and K. Sellegri, New particle formation in coastal new zealand with a focus on open ocean air masses, *Atmospheric Chemistry and Physics Discussions*, 2021, **2021**, 1–34.